

Waveform and Beamforming Design for Intelligent Reflecting Surface Aided Wireless Power Transfer: Single-User and Multi-User Solutions

Zhenyuan Feng,

Member, IEEE, Bruno Clerckx, Senior Member, IEEE and Yang Zhao, Member, IEEE

Abstract

In this paper, we study the waveform and passive beamforming design for intelligent reflecting surface (IRS)-aided wireless power transfer (WPT). Generalized multi-user and low complexity single-user algorithms are derived based on alternating optimization (AO) framework to maximize the weighted sum output DC current, subject to the transmit power constraints and passive beamforming modulus constraints. The input signal waveform and IRS passive beamforming phase shifts are jointly designed as a function of users' individual frequency-selective channel state information (CSI). The energy harvester nonlinearity is explored and two IRS deployment schemes, namely frequency selective IRS (FS-IRS) and frequency flat IRS (FF-IRS), are modeled and analyzed. This paper highlights the fact that IRS can provide an extra passive beamforming gain on output DC power over conventional WPT designs and significantly influence the waveform design by leveraging the benefit of passive beamforming, frequency diversity and energy harvester nonlinearity. Even though FF-IRS exhibits lower output DC current than the ideal FS-IRS, it still achieves substantially increased DC power over conventional WPT designs. Performance evaluations confirm the significant benefits of a joint waveform and passive beamforming design accounting for the energy harvester nonlinearity to boost the performance of single-user and multi-user WPT system.

Index Terms

Wireless power transfer, intelligent reflecting surface, waveform design, passive beamforming, alternating optimization, nonlinear energy harvesting

The authors are with the Department of Electrical and Electronic Engineering, Imperial College London, London SW7 2AZ, U.K. (e-mail: z.feng19, b.clerckx, yang.zhao18@imperial.ac.uk).

I. INTRODUCTION

In the last decade, far field wireless power transfer (WPT) has drawn a great attention because of its potential to energize billions of future autonomous low-power devices. It is deemed as the enabler of the 1G of mobile power networks [1], and numerous applications such as simultaneous wireless information and power transfer (SWIPT), wirelessly powered communication network (WPCNs), Internet of Things (IoT) and wireless powered backscatter communication (WPBC) [2]. The major challenge of far field WPT is to maximize the output DC power or equivalently the end-to-end power transmission efficiency (EPTE) without increasing the transmit power, and for distances over a few to hundreds of meters. The traditional solution to resolve this challenge has focused on the design of efficient energy harvesters, so-called rectennas, with high RF-to-DC conversion efficiency (CE) [3][4][5]. More recently, in addition to rectenna design, a new complementary research direction on signal designs for WPT has gradually emerged [6]. In the past few years, four different signal design strategies have been proposed and optimized.

A *first* strategy is the design of energy *waveforms* to utilize the nonlinearity characteristic of the rectenna and boost jointly the RF-to-RF CE $e_{\text{rf-rf}}$ and the RF-to-DC CE $e_{\text{rf-dc}}$ [7]. Such design originates from the fact that the output of the energy harvester (EH) is a nonlinear function of the rectenna input signal. Hence, the transmit waveform design has a significant influence on the EPTE. It not only affects the RF-to-RF CE and the signal intensity at the input of rectenna, but also the RF-to-DC CE of the rectifier. A stepping stone in such design was made in [7] where a systematic methodology was derived to design and optimize waveforms for WPT. Different from prior non-optimized waveform designs [8], the optimal waveform design in [7] was adapted to the frequency selective channel (with frequency flat channel being a special case) and was rooted in the tradeoff between maximizing $e_{\text{rf-dc}}$ and $e_{\text{rf-rf}}$. Such optimized waveform was shown to provide significant benefits over conventional continuous-wave signal and non-optimized waveforms by leveraging the channel frequency diversity gain and a gain originating from the rectifier nonlinearity. Since the optimal signal design is the solution of computationally involved problems, low complexity methods have been proposed in [9], [10], and have been experimentally validated in [11]. Furthermore, since the channel state information at the transmitter (CSIT) is needed to design the optimal waveform, waveform designs based on limited feedback have been proposed in [12], and experimentally demonstrated in [13].

A *second* strategy is the design of multi antenna *beamforming* to boost the input power of EH and enhance the RF-to-RF CE $e_{\text{rf-rf}}$. Due to the hardware limitation of EH, acquisition of CSIT is challenging. An efficient method was proposed in [14] to overcome this challenge by designing beamforming with limited feedback. Other directive or energy focusing solutions, such as time-reversal techniques [15]

and time-modulated arrays [16], have also been used in WPT system to exploit the real-time antenna beamforming strategies. Beamforming is not limited to the transmitter and can also be used at the receiver subject to a proper design of the combiner scheme [17]. Waveform and beamforming can also be combined into a joint waveform and beamforming design [7], [10], [18] to further boost the output DC power and the range of WPT, as demonstrated experimentally in [19]. Joint waveform and beamforming enables to simultaneously harvest three different gains, namely a beamforming gain, a frequency diversity gain and a gain related to the rectifier nonlinearity, and therefore offers additional opportunities over spatial domain processing/beamforming-only.

A *third* strategy is to design *modulation* for WPT. Different from [7] where energy waveforms consist of deterministic unmodulated multi-carrier signals, modulation induces random fluctuation of the input rectifier signal to increase $e_{\text{rf-dc}}$. For example, real Gaussian modulation outperforms circularly symmetric complex Gaussian (CSCG) modulation despite the same average input power to the rectifier [20]. Similarly, [21] has observed that an on-off keying based modulation strategy outperforms real Gaussian modulation in terms of output DC power.

A *fourth* strategy is to apply phase sweeping *transmit diversity* in multi-antenna settings [22]. Compared to the beamforming strategy, transmit diversity does not rely on CSIT but still increase $e_{\text{rf-dc}}$ and therefore output DC power.

In parallel to the active research area on signal design strategies for WPT, a new paradigm named *intelligent reflecting surfaces* (IRS) has recently attracted the attention of the wireless research community to further boost the efficiency of wireless communications [23], [24], [25], [26], [27]. Compared with the active beamforming of (massive) multi-antenna systems, IRS benefits from the presence of passive beamforming reflection elements (REs) integrated into the propagation environment, which are optimized to adapt the wireless channel so as to be favorable to communication receivers. The key advantages of IRS are the tunability of the phase shifters at each RE (so-called passive beamforming phases), the flexibility of the deployment on arbitrary shaped surfaces and the sustainability due to low cost and power consumption. By collaboratively adjusting the passive beamforming phases, the incident signal is reflected at each RE such that the reflected signals are constructively accumulated at the target receiver to increase the receive signal power, therefore enabling a passive beamforming gain. Nevertheless, in contrast to active antenna arrays where the amplitudes and phases can be adjusted freely at each antenna and at each frequency, REs may be subject to less flexibility due to the passive nature of the IRS and the

hardware constraints. Specifically, the reflection amplitude of the REs is no greater than 1¹. Moreover the IRS is commonly assumed be consistent with frequency-flat in the sense that passive beamforming phases are kept constant across frequencies, (so-called frequency-flat IRS in the sequel). Under those constraints, IRS-assisted wireless communications have focused on single carrier, frequency-flat channel and frequency-flat IRS by jointly designing the active transmit beamforming at the transmitter and passive reflection beamforming at the IRS for single-user [28] and multi-user scenarios [29], [30], [31]. Multi carrier OFDM waveform designs were also studied in some papers using frequency-flat IRS [32], [33].

Aside communications, IRS brings some natural benefits to wireless power since IRS can help increasing the power level at the input of the rectenna. Existing IRS-aided WPT/SWIPT works focus on single tone, frequency-flat IRS, frequency-flat channel and jointly optimize transmit beamforming and passive IRS beamforming phases [34], [35], [36], [37].

The limitation of the existing IRS-aided WPT literature is that the focus is on the spatial domain beamforming-only and that the rectenna nonlinearity has been ignored. Ignoring the rectenna nonlinearity is equivalent to assuming that $e_{\text{rf-dc}}$ is constant and independent of the rectenna input signal power and shape [1], [6]. Unfortunately, such assumption is well documented to be inaccurate and to lead to inefficient designs [11]. Rectenna nonlinearity is indeed known to be a crucial feature to be modeled and accounted for in WPT system design as it significantly influences the WPT (and SWIPT) architecture designs [2], [7]. Modeling the nonlinearity is particularly crucial in the low power regime (below 1mW), which is the primary deployment scenario of WPT in wireless networks. Importantly, the nonlinearity opens the door to more efficient signal strategies, e.g. joint waveform and beamforming, for WPT that significantly enhance the performance over beamforming-only approaches.

In this paper, we derive an efficient IRS-aided WPT design by leveraging the progress made in the past few years on the modeling of the rectenna nonlinearity and its corresponding efficient signal design for WPT on one hand and on IRS on the other hand. Motivated by the significant benefits of a joint waveform and beamforming design to expand the range and the output DC power of WPT [7], [10], [11], this work pushes the limit of IRS-aided WPT by better exploiting the presence of IRS through a joint waveform and beamforming design for both single-user and multi-user deployments.

The contributions of this paper are summarized as follows.

First, we design a novel architecture based on joint waveform and passive beamforming for IRS-aided WPT. We leverage the rectenna nonlinear model of [7] and use it to derive a joint multisine waveform

¹fixed to unity in this paper for maximization of output DC power.

and beamforming optimization framework applicable to both single-user and multi-user IRS-aided WPT deployments. This is the first paper tackling nonlinearity and waveform design in (single-user and multi-user) IRS-aided WPT. By leveraging jointly the frequency and spatial domains, and properly modeling the harvester nonlinearity, the proposed architecture exploits the combined benefits of the passive beamforming gain, the channel frequency selectivity and the rectenna nonlinearity. This contrasts with existing IRS-aided WPT papers [34], [35], [36], [37] whose architecture only benefits from the passive beamforming gain. This also contrasts with existing papers on waveform for WPT [7], [10], whose designs assume active antennas and are therefore not transferable to IRS-aided WPT due to the hardware constraints imposed by IRS.

Second, we develop two different formulations of the joint waveform and beamforming design based on a frequency-selective IRS (FS-IRS) and a frequency-flat IRS (FF-IRS). The FF-IRS assumes that the passive beamforming phases are constant across frequencies, while the FS-IRS is flexible enough to adjust the passive beamforming phases at each frequency of the multisine waveform, which thus renders the weighted sum current problem more difficult to solve. The performance of the FS-IRS always provides an upperbound on the FF-IRS performance and helps assessing how much loss is incurred by constraining the passive beamforming phases to be the same across frequencies. This comparison sheds light on the benefits of developing more advanced IRS hardware enabling frequency-selective passive beamforming phases. This is particularly important in the context of wideband multi-band/carrier WPT since the choice of the passive beamforming phases across frequencies severely influences how much the channel frequency selectivity and the rectenna nonlinearity can be exploited by the waveform design to boost the harvested DC power. This also contrasts with existing IRS-aided WPT papers [34], [35], [36], [37] that ignore such consideration since their designs assume narrowband transmissions and frequency-flat channels.

Third, under the assumption of perfect CSI, we develop an optimization framework for a general multi-user IRS-aided WPT setup based on alternating optimization (AO), successive convex approximation (SCA) and semidefinite relaxation (SDR) to iteratively optimize the IRS passive beamforming phases and waveform weights with the others being fixed. Efficient solution is derived in two subproblems of AO by optimizing one of these variables in closed-form. Conventional WPT waveform optimization strategies mainly rely on Reverse Geometric Program (GP) [7] and Semi-definite Program (SDP)[12], [17], [18]. In contrast, for the FF-IRS, both subproblems of AO are solved by formulating the problem into a standard semidefinite program (SDP) with SCA in an iterative manner. This is different from conventional WPT papers because the output DC current is not only influenced by the waveform weights on each frequency (which is systematically discussed in [7]) but also impacted by the passive beamforming phases in spatial

and frequency domains (which is firstly promoted in this paper). In addition, low complexity solutions are demonstrated in multi-user (MU) and single-user (SU) FS-IRS algorithms with the element-wise updating method and prior determined passive beamforming phases, respectively.

Fourth, numerical results are displayed to validate the theoretical discussion on FS-IRS and FF-IRS WPT algorithms. Although FS-IRS always provides an upperbound performance to FF-IRS, FF-IRS still outperforms conventional WPT papers which emphasizes the significance of passive beamforming designs. Then, FS-IRS brings more opportunities to broadband WPT while FF-IRS is more suitable for narrowband WPT. Both FS-IRS and FF-IRS algorithms can exhibit fast convergence which strongly reveals the effectiveness of the SCA based algorithms. Furthermore, the IRS should be deployed closed to users or BS to obtain larger current region. Moreover, a near-optimal result can be achieved with low-resolution discrete-phase IRS in both FF-IRS and FS-IRS. Numerical results confirm the inefficiency of the linear based model and demonstrate the advancement of IRS-aided WPT on leveraging the nonlinearity of rectenna, waveform weights and passive beamforming phases. In addition, this model can be extended to the multi-antenna case as in [7].

Organization: In section II, we introduce the system model and nonlinear process of the rectenna. The joint optimization problems of generalized MU cases and low complexity SU scenario are discussed in section III. Then, numerical results are illustrated in section IV, followed by the conclusion and future work in section V.

Notations: Vectors and matrices are denoted by bold and lower letters and bold and upper letters, respectively. $(\cdot)^H, (\cdot)^*$ and $(\cdot)^T$ denote conjugate transpose, complex conjugate and transpose. $\|\cdot\|_F$ and $\|\cdot\|$ denote Frobenius norm and 2-norm. We use $|\cdot|$ for absolute value, $\text{Tr}\{\cdot\}$ for trace and $\Re\{\cdot\}$ and $\Im\{\cdot\}$ for real part operators and imaginary part operators. The notation \succeq denotes positive-semidefinite and $\text{diag}\{\mathbf{x}\}$ denotes diagonalization operation with elements of \mathbf{x} in the diagonal. Imaginary unit is denoted as $j = \sqrt{-1}$.

II. SYSTEM MODEL

A. Transmit Signal

As is illustrated in Fig. 1, we consider an IRS-aided downlink single-input-single-output (SISO) WPT system including K single-antenna users, one IRS with L REs and one base station (BS) equipped with single antenna at the transmitter. The multisine waveform at time t is given as

$$x(t) = \Re \left\{ \sum_{n=1}^N s_n e^{j2\pi f_n t} \right\} = \sum_{n=1}^N w_n \cos(2\pi f_n t + \gamma_n) \quad (1)$$

where $s_n = w_n e^{j\gamma_n}$ ($n = 1, \dots, N$) denotes the complex weight of the multisine waveform with w_n and γ_n accounting for the amplitude and phase at frequency n , respectively. For simplicity, we assume that the frequencies are equally spaced, i.e. $f_n = f_0 + n\Delta_f$. The transmit power constraint at the transmitter is written as $\frac{1}{2}\|\mathbf{s}\|^2 \leq P$ with $\mathbf{s} = [s_1, s_2, \dots, s_N]^T \in \mathbb{C}^{N \times 1}$ and $\frac{1}{2}$ referring to the average power of cosine function in (1).

B. Channel Model and Reflection Pattern

The multisine waveform propagates through wireless channels. The channel from the BS to user q , from the BS to the IRS and from the IRS to user q at the frequency n are denoted as $h_{d,q,n}$, $\mathbf{h}_{i,n} \in \mathbb{C}^{L \times 1}$ and $\mathbf{h}_{r,q,n} \in \mathbb{C}^{1 \times L}$, respectively. To facilitate the reading, they are also termed as direct channel, incident channel and reflected channel, respectively. To be specific, we denote the entries of $\mathbf{h}_{i,n}$ as $h_{i,l+(n-1)L}$ and the entries of reflected channel $\mathbf{h}_{r,q,n}$ as $h_{r,q,l+(n-1)L}$ with $\mathbf{h}_{i,n} = [h_{i,1+(n-1)L}, \dots, h_{i,L+(n-1)L}]^T$ and $\mathbf{h}_{r,q,n} = [h_{r,q,1+(n-1)L}, \dots, h_{r,q,L+(n-1)L}]$, respectively. The channels above are assumed quasi-static and the CSIT is assumed to be perfect.

Two IRS deployment scenarios are studied here, namely a frequency-selective IRS (FS-IRS) scenario and a frequency-flat IRS (FF-IRS) scenario. FS-IRS is flexible enough to adjust the passive beamforming phases in different frequencies. In contrast, FF-IRS assumes that passive beamforming phases are constant across frequencies.

1) *FS-IRS*: The complex phasors $e^{j\psi_{l+(n-1)L}}$, $l = 1, 2, \dots, L$, at frequency n are collected on the diagonal entries of the diagonal matrix $\Theta_n \in \mathbb{C}^{L \times L}$ with $\Theta_n = \text{diag}\{e^{j\psi_{1+(n-1)L}}, \dots, e^{j\psi_{L+(n-1)L}}\}$, $\forall n$. We assume that $\psi_{l+(n-1)L} \in [0, 2\pi)$ and $\theta_{l+(n-1)L} = e^{j\psi_{l+(n-1)L}}$, $l = 1, 2, \dots, L$.

2) *FF-IRS*: We design a common set of passive beamforming phases that cater to all subcarriers i.e. $\Theta_n = \Theta = \text{diag}\{e^{j\psi_1}, e^{j\psi_2}, \dots, e^{j\psi_L}\}$, $\forall n$. With $\psi_l \in [0, 2\pi)$, we have $\theta_l = e^{j\psi_l}$, $\forall l$ in the remainder of this paper.

By superposing the auxiliary channel ($\mathbf{h}_{r,q,n} \Theta_n \mathbf{h}_{i,n}$) to the direct channel, we can obtain the composite channel between BS and user q at frequency n as

$$h_{q,n} = h_{d,q,n} + \mathbf{h}_{r,q,n} \Theta_n \mathbf{h}_{i,n}. \quad (2)$$

Remark 1: This paper does not deal with the implementation of FS-IRS but rather use FS-IRS as an upper bound on FF-IRS to assess how much performance could be obtained if FS-IRS could be prototyped by RF engineers. According to [27], the phase shift essentially depends on the reflection

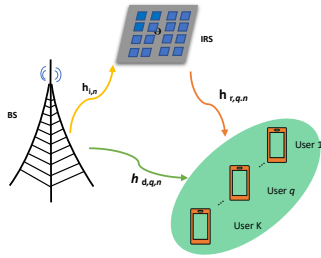


Fig. 1. System model.

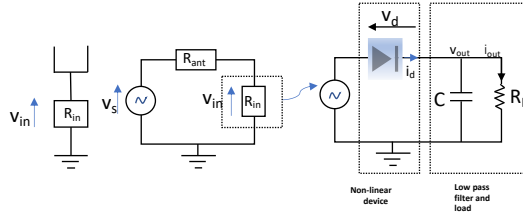


Fig. 2. Antenna equivalent circuit.

coefficient of a reconfigurable impedance. Then, the frequency response of phase shift depends on the frequency response of a particular impedance. Generally, once the circuit topology is fixed, the frequency response is fixed so that it is more complex to implement FS-IRS than FF-IRS. A practical IRS model is illustrated in [38] which emphasizes that the amplitudes and phase of passive beamforming phases vary with the frequencies of transmitted signals. Nevertheless, there is still lack of a general model that can accurately characterize this nonlinear relationship between the practical frequency-dependent passive beamforming phases and nonlinear EH by capturing all factors. Meanwhile, due to the different nature of systems, the objective functions and the receiver architecture, the benefits of FS-IRS over FF-IRS can be much different in WPT and in wideband OFDM communications. This means that any conclusions from IRS-aided communications may not be transferable to WPT. Hence, FF-IRS with unit modulus constraints are adopted in this paper as widely utilized in existing literature [32], [33]. As this is the first work proposing FS-IRS and FF-IRS with nonlinear energy harvester model, we would like to keep the system model as clear and simple as possible such that researchers can understand the fundamental benefits of the two proposed strategies and carry on its study in more practical model in the future.

C. Receive Signal

The received signal at user q of time t for FS-IRS can be expressed as²

$$y_q(t) = \Re \left\{ \sum_{n=1}^N (h_{d,q,n} + \mathbf{h}_{r,q,n} \Theta_n \mathbf{h}_{i,n}) s_n e^{j2\pi f_n t} \right\} \quad (3)$$

where $q=1,2,\dots,K$ and $y_q(t)$ is the input of the rectenna which is discussed in the next part. In FF-IRS, Θ_n is replaced with $\Theta, \forall n$.

D. Rectenna model

We revisit the nonlinear process of the energy receiver in [7]. Consider a simple tractable model of the rectifier which is demonstrated in Fig. 2. The impinging received signal $y_q(t)$ has a average power $P_r =$

²In this paper, we ignore the signals which are reflected by IRS for two or more times due to substantial path loss.

$\mathcal{E}\{|y_q(t)|^2\}$. The receive antenna is assumed to be a lossless antenna which can be modeled as a voltage source $v_s(t)$. Then, the rectenna architecture can be seen as a voltage source $v_s(t)$ connected with a rectifier input impedance $Z_{\text{in}} = R_{\text{in}} + jX_{\text{in}}$ and an antenna impedance $Z_{\text{ant}} = R_{\text{ant}} + jX_{\text{ant}}$. Under the assumption of lossless antenna and perfect matching ($R_{\text{ant}} = R_{\text{in}}, X_{\text{ant}} = -X_{\text{in}}$), the receive power P_r is completely transferred to rectenna impedance which builds the relation between P_r and $v_{\text{in}}(t)$ such that $P_r = \mathcal{E}\{|y_q(t)|^2\} = \mathcal{E}\{|y_q(t)|^2\} \frac{R_{\text{ant}}}{R_{\text{in}}} = \frac{\mathcal{E}\{|v_{\text{in}}(t)|^2\}}{R_{\text{in}}}$. Under the assumption of perfect matching, we have $v_s(t) = 2v_{\text{in}}(t)$. Hence, $v_{\text{in}}(t)$ can be associated with the received signal $y_q(t)$ with $v_{\text{in}}(t) = y_q(t)\sqrt{R_{\text{ant}}}$ [7]. To have a deep view of the rectifier DC output current i_{out} , we focus on the diode I-V characteristic $i_d(t) = i_s(e^{\frac{v_{\text{in}}(t) - v_{\text{out}}(t)}{n'v_t}} - 1)$ where i_s, n' and v_t are the reverse bias saturation current, diode ideal factor and thermal voltage, respectively. The diode nonlinearity is rooted in the term $e^{\frac{v_d(t)}{n'v_t}}$. [7][39] illustrates the significance of the higher order (≥ 4) truncation of the Taylor series for the term $e^{\frac{v_d(t)}{n'v_t}}$ through $i_d(t) \approx \sum_{i=0, \text{even}}^{n_0} \beta_i R_{\text{ant}}^{i/2} y_q(t)^i$ with $\beta_i \triangleq i_s / i! (n'v_t)^i$. After the low pass filter (LPF), the approximated output DC current i_{out} is given by

$$i_{\text{out}} = \mathcal{E}\{i_d(t)\} \approx \sum_{i=0, \text{even}}^{n_0} \beta_i R_{\text{ant}}^{i/2} \mathcal{E}\{y_q(t)^i\}. \quad (4)$$

To get a tractable analytical model, one can truncate to $n_0 = 4$ while retaining the main source of nonlinearity as part of the fourth order term. Higher order analysis can be found in [7][39]. Interestingly, the 2nd order term is essentially the linear based rectenna model which is widely addressed in existed IRS-aided WPT/SWIPT papers [34], [35], [36], [37] and is confirmed to be an inefficient and inaccurate in Section IV-A (Fig. 8).³

E. Discussion on Multi-Antenna Scenario

The main contribution of this paper is to maximize the output DC power by leveraging the frequency diversity gain, the passive beamforming gain and the gain from EH nonlinearity. The active beamforming will not fundamentally change the observation and novelty of this paper. To keep explanation simpler without being overwhelmed by the variables of a multi-antenna scenario, multi-user SISO transmission model is chosen in our paper. However, it is easy to scale to multi-antenna system with the same AO framework in the next section and the benefits of transmit active beamforming is shown in Fig. 17.

III. JOINT DESIGN OF WPT WAVEFORM AND REFLECTION ELEMENTS FOR MULTI-USER SCENARIO

The purpose of the multi-user designs is to jointly optimize the frequency domain complex weights of the waveform and passive beamforming phases of IRS to maximize the K -user weighted sum output

³In addition, as a fundamental property in I-V characteristic, the diode should operate over the nonlinear region with appropriate signal power. If the input power is too high, the diode will perform in linear region and (4) does not hold.

DC current, subject to the input power constraint ($\frac{1}{2}\|\mathbf{s}\|^2 \leq P$) as well as the unit modulus constraints ($|\theta_{l+(n-1)L}| = 1$). Using the model of (4) and truncating to order 4, i.e. $n_0 = 4$, the approximated DC current of user q is $i_{\text{dc},q} = \sum_{n, \text{ even}, n \geq 2}^4 \beta_n R_{\text{ant}}^{n/2} \mathcal{E}\{y_q(t)^n\}$. $i_{\text{dc},q}$ can be found as

$$i_{\text{dc},q} = k_2 \mathcal{E}\{y_q(t)^2\} + k_4 \mathcal{E}\{y_q(t)^4\} \quad (5)$$

where $k_2 = \beta_2 R_{\text{ant}} = 0.17$ and $k_4 = \beta_4 R_{\text{ant}}^2 = 957.25$ (assuming that $i_s = 5\mu\text{A}$, $n' = 1.05$ and $v_t = 25.86\text{mV}$). Then, $\mathcal{E}\{y(t)^2\}$, $\mathcal{E}\{y(t)^4\}$ and the DC output current $i_{\text{dc},q}$ are calculated as

$$\mathcal{E}\{y_q(t)^2\} = \frac{1}{2} \sum_{n=1}^N s_n^* h_{q,n}^* h_{q,n} s_n, \quad (6)$$

$$\mathcal{E}\{y_q(t)^4\} = \frac{3}{8} \sum_{\substack{n_1, n_2, n_3, n_4 \\ n_1 + n_3 = n_2 + n_4}} s_{n_1}^* h_{q,n_1}^* h_{q,n_2} s_{n_2} s_{n_3}^* h_{q,n_3}^* h_{q,n_4} s_{n_4}, \quad (7)$$

$$i_{\text{dc},q}(\mathbf{s}, \{\Theta_n\}_{n=1}^N) = \frac{1}{2} k_2 \sum_{n=1}^N s_n^* h_{q,n}^* h_{q,n} s_n + \frac{3}{8} k_4 \sum_{\substack{n_1, n_2, n_3, n_4 \\ n_1 + n_3 = n_2 + n_4}} s_{n_1}^* h_{q,n_1}^* h_{q,n_2} s_{n_2} s_{n_3}^* h_{q,n_3}^* h_{q,n_4} s_{n_4}, \quad (8)$$

respectively, where the composite channel $h_{q,n}$ is given by (2)⁴. The corresponding problem can be formulated as a weighted sum of DC current

$$\max_{\mathbf{s}, \{\Theta_n\}_{n=1}^N} \sum_{q=1}^K \xi_q i_{\text{dc},q}(\mathbf{s}, \{\Theta_n\}_{n=1}^N) \quad (9a)$$

$$\text{s.t.} \quad \|\mathbf{s}\|^2 \leq 2P, \quad (9b)$$

$$|\theta_{l+(n-1)L}| = 1, n = 1, 2, \dots, N, l = 1, 2, \dots, L \quad (9c)$$

where ξ_q is the weight for the q th user.

For the alternating optimization algorithms in the next sections, the passive beamforming $\{\Theta_n^{(i)}\}_{n=1}^N$ and the waveform weights $\mathbf{s}^{(i-1)}$ are sequentially updated in each iteration until convergence.

⁴When it comes to the multi-antenna scenario, the objective function (8) becomes $i_{\text{dc}}(\mathbf{s}, \Theta) = \frac{1}{2} k_2 \sum_{n=1}^N \mathbf{s}_n^H \mathbf{h}_{k,n}^H \mathbf{h}_{k,n} \mathbf{s}_n + \frac{3}{8} k_4 \sum_{\substack{n_1, n_2, n_3, n_4 \\ n_1 + n_3 = n_2 + n_4}} \mathbf{s}_{n_1}^H \mathbf{h}_{k,n_1}^H \mathbf{h}_{k,n_2} \mathbf{s}_{n_2} \mathbf{s}_{n_3}^H \mathbf{h}_{k,n_3}^H \mathbf{h}_{k,n_4} \mathbf{s}_{n_4}$ where $\mathbf{s}_n = [s_{1+(n-1)M_t}, s_{2+(n-1)M_t}, \dots, s_{M_t+(n-1)M_t}]$ and $\mathbf{h}_{k,n} = \mathbf{h}_{d,q,n} + \mathbf{h}_{r,q,n} \Theta_n \mathbf{H}_{i,n} \in \mathbb{C}^{1 \times M_t}$.

$$\mathbf{D}_q = \begin{pmatrix}
\mathbf{z}_{q,1}\mathbf{z}_{q,1}^H & \mathbf{z}_{q,1}\mathbf{z}_{q,2}^H & \mathbf{z}_{q,1}\mathbf{z}_{q,3}^H & \mathbf{z}_{q,1}\mathbf{z}_{q,4}^H & \cdots & \mathbf{z}_{q,1}\mathbf{z}_{q,N}^H \\
\mathbf{z}_{q,2}\mathbf{z}_{q,1}^H & \mathbf{z}_{q,2}\mathbf{z}_{q,2}^H & \mathbf{z}_{q,2}\mathbf{z}_{q,3}^H & \mathbf{z}_{q,2}\mathbf{z}_{q,4}^H & \cdots & \vdots \\
\mathbf{z}_{q,3}\mathbf{z}_{q,1}^H & \mathbf{z}_{q,3}\mathbf{z}_{q,2}^H & \mathbf{z}_{q,3}\mathbf{z}_{q,3}^H & \mathbf{z}_{q,3}\mathbf{z}_{q,4}^H & \cdots & \vdots \\
\mathbf{z}_{q,4}\mathbf{z}_{q,1}^H & \mathbf{z}_{q,4}\mathbf{z}_{q,2}^H & \mathbf{z}_{q,4}\mathbf{z}_{q,3}^H & \mathbf{z}_{q,4}\mathbf{z}_{q,4}^H & \cdots & \vdots \\
\vdots & \vdots & \vdots & \vdots & \ddots & \vdots \\
\mathbf{z}_{q,N}\mathbf{z}_{q,1}^H & \cdots & \cdots & \cdots & \cdots & \mathbf{z}_{q,N}\mathbf{z}_{q,N}^H
\end{pmatrix}$$

$k = 1$ (points to the second column)
 $k = 0$ (points to the first column)
 $k = -1$ (points to the first row)

Fig. 3. $\mathbf{D}_{q,0}$ is the sum of red block diagonal, $\mathbf{D}_{q,1}$ is the sum of yellow block diagonal and $\mathbf{D}_{q,-1}$ is the sum of green block diagonal in the above matrix.

A. Passive Beamforming for Multi-User FF-IRS

In FF-IRS, we optimize L passive beamforming phases which are constrained to be constant across all N frequencies. To build this weighted sum current subproblem on passive beamforming phases, we denote $\mathbf{v}_{q,n} = \begin{bmatrix} \text{diag}\{\mathbf{h}_{r,q,n}\}\mathbf{h}_{i,n} \\ h_{d,q,n} \end{bmatrix} \in \mathbb{C}^{(L+1) \times 1}$. Denote $\boldsymbol{\theta} = [\theta_1, \theta_2, \dots, \theta_L, m_1] \in \mathbb{C}^{1 \times (L+1)}$ with m_1 referring to an auxiliary variable. Then $(h_{d,q,n} + \mathbf{h}_{r,q,n}\boldsymbol{\Theta}\mathbf{h}_{i,n})s_n = \boldsymbol{\theta}\mathbf{v}_{q,n}s_n$ and we let $\mathbf{z}_{q,n} = \mathbf{v}_{q,n}s_n$ which is grouped into $\mathbf{z}_q = [\mathbf{z}_{q,1}^T, \mathbf{z}_{q,2}^T, \dots, \mathbf{z}_{q,N}^T]^T \in \mathbb{C}^{(L+1)N \times 1}$. The $i_{dc,q}(\mathbf{s}, \{\boldsymbol{\Theta}_n\}_{n=1}^N)$ in (9a) can be equivalently rewritten as $i_{dc,q}(\boldsymbol{\theta})$ below

$$i_{dc,q}(\boldsymbol{\theta}) = \frac{1}{2}k_2 \sum_{n=1}^N \boldsymbol{\theta}\mathbf{z}_{q,n}\mathbf{z}_{q,n}^H\boldsymbol{\theta}^H + \frac{3}{8}k_4 \sum_{\substack{n_1, n_2, n_3, n_4 \\ n_1 + n_3 = n_2 + n_4}} \boldsymbol{\theta}\mathbf{z}_{q,n_1}\mathbf{z}_{q,n_2}^H\boldsymbol{\theta}^H\boldsymbol{\theta}\mathbf{z}_{q,n_3}\mathbf{z}_{q,n_4}^H\boldsymbol{\theta}^H. \quad (10)$$

To transform (10) into a more compact form, we define $N(L+1)$ -by- $N(L+1)$ matrix \mathbf{D}_q and $(L+1)$ -by- $(L+1)$ matrices $\mathbf{D}_{q,k}$ where $\mathbf{D}_q = \mathbf{z}_q\mathbf{z}_q^H$ which is shown in Fig. 3. $k = 0$ refers to the index of the main block diagonal of \mathbf{D}_q . $k \in \{1, \dots, N-1\}$ denotes the index of the k th block diagonal above the main block diagonal of the matrix \mathbf{D}_q . $k \in \{-(N-1), \dots, -1\}$ denotes the index of the $|k|$ th block diagonal below the main block diagonal. Matrix $\mathbf{D}_{q,k}$ is obtained by summing the block matrices of the k th block diagonal of \mathbf{D}_q e.g. $\mathbf{D}_{q,0} = \mathbf{z}_{q,1}\mathbf{z}_{q,1}^H + \mathbf{z}_{q,2}\mathbf{z}_{q,2}^H + \cdots + \mathbf{z}_{q,N}\mathbf{z}_{q,N}^H$, $\mathbf{D}_{q,1} = \mathbf{z}_{q,1}\mathbf{z}_{q,2}^H + \mathbf{z}_{q,2}\mathbf{z}_{q,3}^H + \cdots + \mathbf{z}_{q,N-1}\mathbf{z}_{q,N}^H$ and $\mathbf{D}_{q,N-1} = \mathbf{z}_{q,1}\mathbf{z}_{q,N}^H$. Luckily, we can get a compact form of (10) for the q th user as

$$i_{dc,q}(\boldsymbol{\theta}) = \frac{1}{2}k_2\boldsymbol{\theta}\mathbf{D}_{q,0}\boldsymbol{\theta}^H + \frac{3}{8}k_4\boldsymbol{\theta}\mathbf{D}_{q,0}\boldsymbol{\theta}^H(\boldsymbol{\theta}\mathbf{D}_{q,0}\boldsymbol{\theta}^H)^H + \frac{3}{4}k_4 \sum_{k=1}^{N-1} \boldsymbol{\theta}\mathbf{D}_{q,k}\boldsymbol{\theta}^H(\boldsymbol{\theta}\mathbf{D}_{q,k}\boldsymbol{\theta}^H)^H. \quad (11)$$

Then, we formulate weighted sum current problem which is subject to the unit modulus constraints

$$\max_{\boldsymbol{\theta}} \left\{ \sum_{q=1}^K \xi_q i_{dc,q}(\boldsymbol{\theta}) : |\theta_l| = 1, l = 1, 2, \dots, L \right\}. \quad (12)$$

However, this problem is a quartic polynomial which is NP-hard in general. To unveil this problem, we introduce auxiliary variable $d_{q,k}$ where $k \in [0, \dots, N-1]$ and $d_{q,k} = \boldsymbol{\theta} \mathbf{D}_{q,k} \boldsymbol{\theta}^H$. However, for $k \neq 0$, $\mathbf{D}_{q,k}$ is non-Hermitian matrix and the problem becomes a quadratic polynomial which is also NP-hard. To deal with this, we introduce a rank-1 positive semidefinite matrix variable $\mathbf{X} = \boldsymbol{\theta}^H \boldsymbol{\theta} \in \mathbb{C}^{(L+1) \times (L+1)}$ to linearize the problem with $d_{q,k} = \boldsymbol{\theta} \mathbf{D}_{q,k} \boldsymbol{\theta}^H = \text{Tr}\{\mathbf{D}_{q,k} \boldsymbol{\theta}^H \boldsymbol{\theta}\} = \text{Tr}\{\mathbf{D}_{q,k} \mathbf{X}\}$. After defining $\mathbf{d}_q = [d_{q,0}, d_{q,1}, \dots, d_{q,N-1}]^T$, $\mathbf{K}_0 = \text{diag}\{\frac{3}{8}k_4, \frac{3}{4}k_4, \dots, \frac{3}{4}k_4\} \succeq 0$ and the diagonal element of \mathbf{X} as $\mathbf{X}_{l',l'}$ with $l' = 1, 2, \dots, L+1$, problem (12) can be transformed to an equivalent problem as

$$\min_{t_0, \{\mathbf{d}_q\}_{q=1}^K} t_0 \quad (13a)$$

$$\text{s.t.} \quad \sum_{q=1}^K \xi_q \left(-\frac{1}{2} k_2 d_{q,0} - \mathbf{d}_q^H \mathbf{K}_0 \mathbf{d}_q \right) - t_0 \leq 0, \quad (13b)$$

$$\text{Tr}\{\mathbf{D}_{q,k} \mathbf{X}\} = d_{q,k}, \forall q, k, \quad (13c)$$

$$\mathbf{X}_{l',l'} = 1, \forall l', \quad (13d)$$

$$\mathbf{X} \succeq 0, \quad (13e)$$

$$\text{rank}(\mathbf{X}) = 1 \quad (13f)$$

which is still a non-convex problem because of the existence of rank constraint (13f). We apply SDR to relax (13f) and focus on relaxed problems (13a)-(13e). As the term $\mathbf{d}_q^H \mathbf{K}_0 \mathbf{d}_q$ in (13b) is a non-convex quadratic constraint, SCA can be applied to address this problem to approximate the non-convex constraint into a convex constraint and solve the approximated convex problem iteratively. At iteration i , the optimal $\mathbf{d}_q^{(i)}$ can be approximated by the optimal $\mathbf{d}_q^{(i-1)}$ via Taylor expansion [40]. With $f(\mathbf{d}_q) = \mathbf{d}_q^H \mathbf{K}_0 \mathbf{d}_q$, we have

$$f\left(\mathbf{d}_q, \mathbf{d}_q^{(i-1)}\right) \triangleq 2\Re\left\{\mathbf{d}_q^{(i-1)H} \mathbf{K}_0 \mathbf{d}_q\right\} - \mathbf{d}_q^{(i-1)H} \mathbf{K}_0 \mathbf{d}_q^{(i-1)}. \quad (14)$$

From [41], (14) has the pattern that $f(\mathbf{d}_q^{(i)}, \mathbf{d}_q^{(i)}) = f(\mathbf{d}_q^{(i)}) \geq f(\mathbf{d}_q^{(i)}, \mathbf{d}_q^{(i-1)})$. Accordingly, non-convex constraint (13b) has the property that $\sum_{q=1}^K \xi_q \left(-\frac{1}{2} k_2 d_{q,0} - f(\mathbf{d}_q^{(i)}) \right) \leq \sum_{q=1}^K \xi_q \left(-\frac{1}{2} k_2 d_{q,0} - f(\mathbf{d}_q^{(i)}, \mathbf{d}_q^{(i-1)}) \right) \leq t_0$. Since inequation $\sum_{q=1}^K \xi_q \left(-\frac{1}{2} k_2 d_{q,0} - f(\mathbf{d}_q^{(i)}, \mathbf{d}_q^{(i-1)}) \right) \leq t_0$ is a convex constraint at iteration i , relaxed

problems (13a)-(13e) can be formulated as a standard SDP as

$$\min_{t_0, \mathbf{d}_q, \mathbf{X} \succeq 0} t_0 \quad (15a)$$

$$\text{s.t.} \quad \sum_{q=1}^K \xi_q \left(-\frac{1}{2} k_2 d_{q,0} - f(\mathbf{d}_q, \mathbf{d}_q^{(i-1)}) \right) - t_0 \leq 0, \quad (15b)$$

$$(13c), (13d) \text{ and } (13e). \quad (15c)$$

By substituting (13c) into (15b), it follows that

$$\min \quad \text{Tr}\{\mathbf{K}_1 \mathbf{X}\} \quad (16a)$$

$$\text{s.t.} \quad \mathbf{X}_{l', l'} = 1, l' = 1, 2, \dots, L+1, \quad (16b)$$

$$\mathbf{X} \succeq 0 \quad (16c)$$

where $\mathbf{K}_1 = \mathbf{J}_1 + \mathbf{J}_1^H$ is a Hermitian matrix and

$$\mathbf{J}_1 = \sum_{q=1}^K \xi_q \left(-\frac{k_2}{4} \mathbf{D}_{q,0} - \frac{3}{8} k_4 d_{q,0}^{(i-1)} \mathbf{D}_{q,0} - \frac{3}{4} k_4 \sum_{k=1}^{N-1} d_{q,k}^{(i-1)*} \mathbf{D}_{q,k} \right). \quad (17)$$

This standard SDP problem (16) can be solved by invoking existing softwares, e.g., CVX MATLAB [42]. Denoting the solution as \mathbf{X}^* , if $\text{rank}(\mathbf{X}^*) = 1$, the SDR is tight and \mathbf{X}^* is a stationary point of (16) so that a local optimal solution can be extracted by $\mathbf{X}^* = \boldsymbol{\theta}^{*(i)} \boldsymbol{\theta}^{H*(i)}$ [43]. If $\text{rank}(\mathbf{X}^*) > 1$, we can only use the Gaussian randomization method in [44], [45] to extract a suboptimal rank-1 solution $\boldsymbol{\theta}^{(i)} = [\theta_1^{(i)}, \theta_2^{(i)}, \dots, \theta_L^{(i)}, m_1^{(i)}]$, retrieve the phase shifts by $\boldsymbol{\theta}^{*(i)} = \boldsymbol{\theta}^{(i)} / m_1^{(i)}$ and group the first L elements into the diagonal of $\boldsymbol{\Theta}^{*(i)} = \text{diag}\{\boldsymbol{\theta}^{*(i)}[1:L]\}$. Then, we have the composite channel $h_{q,n} = (h_{d,q,n} + \mathbf{h}_{r,q,n} \boldsymbol{\Theta}^{*(i)} \mathbf{h}_{i,n})$.

Remark 2: Note that different from [34] where a predefined minimum harvested power threshold is addressed, problem (16) is a standard SDP in each iteration with only unit modulus constraint. The known approximation accuracy for this complex constant modulus problem is $\pi/4$ which guarantees that a good approximation can be found if we have a rank-1 solution [43]. When we evaluated the results in Section IV, we found that all channel realizations generated a rank-1 \mathbf{X}^ . This is particularly important since Algorithm 1 is guaranteed to provide a stationary point for problem (9) with a rank-1 solution in the simulations (see Appendix B). Even though the performance is degraded by the Gaussian randomization method later, the performance loss is still negligible if \mathbf{X}^* is rank-1 for all tested channels [25].*

B. Passive Beamforming for Multi-User FS-IRS

In MU FS-IRS, different from problem (12), we aim to maximize the weighted sum current subject to NL unit modulus constraints and the problem can be written as

$$\max_{\{\boldsymbol{\Theta}_n\}_{n=1}^N} \left\{ \sum_{q=1}^K \xi_q i_{\text{dc},q}(\{\boldsymbol{\Theta}_n\}_{n=1}^N) : |\theta_{l+(n-1)L}| = 1, n \in 1, 2, \dots, N, l \in 1, 2, \dots, L \right\}. \quad (18)$$

To obtain a compact form, we define $\mathbf{v}_{q,n} = \begin{bmatrix} \text{diag}\{\mathbf{h}_{r,q,n}\} \mathbf{h}_{i,n} \\ h_{d,q,n} \end{bmatrix} \in \mathbb{C}^{(L+1) \times 1}$. We denote $\boldsymbol{\theta}_n = [\theta_{1+(n-1)L}, \dots, \theta_{L+(n-1)L}, m_n] \in \mathbb{C}^{1 \times (L+1)}$, $\forall n$ with m_n referring to an auxiliary variable. We have $(h_{d,q,n} + \mathbf{h}_{r,q,n} \boldsymbol{\Theta}_n \mathbf{h}_{i,n}) s_n = \boldsymbol{\theta}_n \mathbf{v}_{q,n} s_n$. Denote $\mathbf{z}_{q,n} = \mathbf{v}_{q,n} s_n \in \mathbb{C}^{(L+1) \times 1}$ which is grouped into $\mathbf{z}_q = [\mathbf{z}_{q,1}^T, \mathbf{z}_{q,2}^T, \dots, \mathbf{z}_{q,N}^T]^T \in \mathbb{C}^{(L+1)N \times 1}$. (8) can be rewritten as

$$i_{\text{dc},q}(\{\boldsymbol{\theta}_n\}_{n=1}^N) = \frac{1}{2} k_2 \sum_{n=1}^N \boldsymbol{\theta}_n \mathbf{z}_{q,n} \mathbf{z}_{q,n}^H \boldsymbol{\theta}_n^H + \frac{3}{8} k_4 \sum_{\substack{n_1, n_2, n_3, n_4 \\ n_1 + n_3 = n_2 + n_4}} \boldsymbol{\theta}_n \mathbf{z}_{q,n_1} \mathbf{z}_{q,n_2}^H \boldsymbol{\theta}_n^H \boldsymbol{\theta}_n \mathbf{z}_{q,n_3} \mathbf{z}_{q,n_4}^H \boldsymbol{\theta}_n^H. \quad (19)$$

To formulate (19) into a more tractable compact form, we denote $\boldsymbol{\theta} = [\boldsymbol{\theta}_1, \dots, \boldsymbol{\theta}_N] \in \mathbb{C}^{1 \times N(L+1)}$ and define $(L+1)N$ -by- $(L+1)N$ matrices \mathbf{E}_q and $\mathbf{E}_{q,k}$ with $\mathbf{E}_q = \mathbf{z}_q \mathbf{z}_q^H$. $k=0$ denotes the index of the main block diagonal in \mathbf{E}_q . $k \in \{1, \dots, N-1\}$ denotes the index of the k th block diagonal above main diagonal of \mathbf{E}_q . $k \in \{-(N-1), \dots, -1\}$ denotes the index of the $|k|$ th block diagonal below the main block diagonal. $\mathbf{E}_{q,k}$ is obtained by retaining the k th block diagonal of \mathbf{E}_q and setting other block matrices as $\mathbf{0}_{(L+1) \times (L+1)}$. Then, the output current for user q can be equivalently written as

$$i_{\text{dc},q}(\boldsymbol{\theta}) = \frac{1}{2} k_2 \boldsymbol{\theta} \mathbf{E}_{q,0} \boldsymbol{\theta}^H + \frac{3}{8} k_4 \boldsymbol{\theta} \mathbf{E}_{q,0} \boldsymbol{\theta}^H (\boldsymbol{\theta} \mathbf{E}_{q,0} \boldsymbol{\theta}^H)^H + \frac{3}{4} k_4 \sum_{k=1}^{N-1} \boldsymbol{\theta} \mathbf{E}_{q,k} \boldsymbol{\theta}^H (\boldsymbol{\theta} \mathbf{E}_{q,k} \boldsymbol{\theta}^H)^H. \quad (20)$$

To linearize the quartic function (20), we take $\boldsymbol{\theta} \mathbf{E}_{q,k} \boldsymbol{\theta}^H = e_{q,k}$ which is collected into $\mathbf{e}_q = [e_{q,0}, e_{q,1}, \dots, e_{q,N-1}]^T$. (20) can be written as $i_{\text{dc},q}(\mathbf{e}_q) = \frac{1}{2} k_2 e_{q,0} + \mathbf{e}_q^H \mathbf{K}_0 \mathbf{e}_q$. The problem can be formulated as

$$\min_{t_1, \{\mathbf{e}_q\}_{q=1}^K} t_1 \quad (21a)$$

$$\text{s.t.} \quad \sum_{q=1}^K \xi_q \left(-\frac{1}{2} k_2 e_{q,0} - \mathbf{e}_q^H \mathbf{K}_0 \mathbf{e}_q \right) - t_1 \leq 0, \quad (21b)$$

$$\boldsymbol{\theta} \mathbf{E}_{q,k} \boldsymbol{\theta}^H = e_{q,k}, \forall q, k, \quad (21c)$$

$$|\theta_{l+(n-1)L}| = 1, \forall n, l. \quad (21d)$$

We still approximate the non-convex constraint (21b) iteratively by the SCA which is similar with that in Section III-A and the problem can be reformulated as

$$\begin{aligned} \min_{\boldsymbol{\theta}} \quad & \boldsymbol{\theta} \mathbf{K}_2 \boldsymbol{\theta}^H \\ \text{s.t.} \quad & (21c) \text{ and } (21d) \end{aligned} \quad (22)$$

where $\mathbf{K}_2 = \mathbf{J}_2 + \mathbf{J}_2^H$ is a Hermitian matrix and \mathbf{J}_2 is

$$\mathbf{J}_2 = \sum_{q=1}^K \xi_q \left(-\frac{k_2}{4} \mathbf{E}_{q,0} - \frac{3}{8} k_4 e^{(i-1)} \mathbf{E}_{q,0} - \frac{3}{4} k_4 \sum_{k=1}^{N-1} [e_{q,k}^{(i-1)}]^* \mathbf{E}_{q,k} \right). \quad (23)$$

If we apply the same approach as in Section III-A to problem (22), that is, by denoting $\mathbf{X} = \boldsymbol{\theta}^H \boldsymbol{\theta}$ and formulating problem (22) into a SDP, solving this intricate SDP will render a complexity around $O((NL)^6)$ which demonstrates low feasibility for large number of frequencies. To tackle this issue, here, we illustrate a low complexity strategy to optimize the NL elements in $\boldsymbol{\theta}$ with a complexity around $O((NL)^2)$.

Element-Wise Updating Method: Element-Wise Updating Method (EWU) sequentially optimizes $N(L+1)$ variables (NL passive beamforming phases variables and L auxiliary variables) in $\boldsymbol{\theta}$ which is also applied in [46] and [47]. To facilitate the reading, in this method, we denote $\mathbf{K} = -\mathbf{K}_2$ and the element at the i th row and the j th column of \mathbf{K} as $k_{i,j}, i = 1, 2, \dots, N(L+1), j = 1, 2, \dots, N(L+1)$. In addition, we denote the m th variable in $\boldsymbol{\theta}$ as θ_m in this part for simplicity (instead of $\theta_{l+(n-1)L}$ in the preceding discussion). minimization of $\boldsymbol{\theta} \mathbf{K}_2 \boldsymbol{\theta}^H$ in problem (22) becomes maximization of $\boldsymbol{\theta} \mathbf{K} \boldsymbol{\theta}^H$ with the same unit modulus constraints (21d). Since θ_m is updated with other $N(L+1) - 1$ elements in $\boldsymbol{\theta}$ being fixed, $\boldsymbol{\theta} \mathbf{K} \boldsymbol{\theta}^H$ can be written as an element-wise function $f(\theta_m)$ below

$$f(\theta_m) = \theta_m k_{m,m} \theta_m^* + \sum_{j=1, j \neq m}^{N(L+1)} \theta_m k_{m,j} \theta_j^* + \sum_{i=1, i \neq m}^{N(L+1)} \theta_i k_{i,m} \theta_m^* + \sum_{i \neq m, j \neq m} \theta_i k_{i,j} \theta_j \quad (24)$$

where $m = 1, \dots, N(L+1)$.

Due to the fact that \mathbf{K} is a Hermitian matrix, we substitute $k_{i,j} = k_{j,i}^*$ and yield

$$f(\theta_m) = \theta_m k_{m,m} \theta_m^* + 2\Re \left\{ \sum_{j=1, j \neq m}^{N(L+1)} \theta_m k_{m,j} \theta_j^* \right\} + \sum_{i \neq m, j \neq m} \theta_i k_{i,j} \theta_j. \quad (25)$$

In order to optimize θ_m , we abandon other irrelevant elements. The objective function $g(\theta_m)$ becomes

$$g(\theta_m) = k_{m,m} |\theta_m^*|^2 + 2\Re \left\{ \sum_{j=1, j \neq m}^{N(L+1)} \theta_m k_{m,j} \theta_j^* \right\}. \quad (26)$$

Since $|\theta_m^*|^2 = 1$, maximizing $g(\theta_m)$ is to maximize the term $\Re \left\{ \sum_{j=1, j \neq m}^{N(L+1)} \theta_m k_{m,j} \theta_j^* \right\}$. After denoting

$\sum_{j=1, j \neq m}^{N(L+1)} k_{m,j} \theta_j^* = C_m$, the optimal θ_m^* is

$$\angle \theta_m^* = -\angle C_m, \theta_m^* = e^{-j \angle C_m}. \quad (27)$$

Therefore, θ_m^* can be determined one by one until all $N(L+1)$ variables are updated.

After this SCA based EWU method, similarly, the composite channel for user q is obtained by grouping the first L elements of $\boldsymbol{\theta}_n$ into the diagonal matrix $\boldsymbol{\Theta}_n^{*(i)} = \text{diag}\{\boldsymbol{\theta}_n^{*(i)}[1:L]\}$ and substituting the $\boldsymbol{\Theta}_n^{*(i)}$ into the auxiliary channel to get $h_{q,n} = h_{d,q,n} + \mathbf{h}_{r,q,n} \boldsymbol{\Theta}_n^{*(i)} \mathbf{h}_{i,n}$.

C. Waveform Design for Multi-User FF-IRS and Multi-User FS-IRS

In this section, we aim to maximize the weighted sum current subject to the power constraint at the transmitter for the composite channel $h_{q,n}$ obtained in the previous sections by optimizing the waveform weights at different frequencies. To formulate this subproblem into a compact form, we introduce N -by- N matrices $\mathbf{B}_q = \mathbf{h}_q^H \mathbf{h}_q$ with $\mathbf{h}_q = [h_{q,1}, h_{q,2}, \dots, h_{q,n}]$, which is shown in Fig. 4. $k \in \{1, \dots, N-1\}$ denotes the index of the k th diagonal above the main diagonal (with index $k=0$) of the matrix \mathbf{B}_q . $k \in \{-(N-1), \dots, -1\}$ denotes the index of the $|k|$ th diagonal below the main diagonal. $\mathbf{B}_{q,k}$ is obtained by retaining the k th diagonal of \mathbf{B}_q with other entries being zeros. The compact form of the output current at the q th user $i_{\text{dc},q}(\mathbf{s})$ can be recast as

$$i_{\text{dc},q}(\mathbf{s}) = \frac{1}{2}k_2 \mathbf{s}^H \mathbf{B}_{q,0} \mathbf{s} + \frac{3}{8}k_4 \mathbf{s}^H \mathbf{B}_{q,0} \mathbf{s} (\mathbf{s}^H \mathbf{B}_{q,0} \mathbf{s})^H + \frac{3}{4}k_4 \sum_{k=1}^{N-1} \mathbf{s}^H \mathbf{B}_{q,k} \mathbf{s} (\mathbf{s}^H \mathbf{B}_{q,k} \mathbf{s})^H. \quad (28)$$

The weighted sum current of all users can be written as $\sum_{q=1}^K \xi_q i_{\text{dc},q}(\mathbf{s})$. Denote the auxiliary variable $b_{q,k} = \mathbf{s}^H \mathbf{B}_{q,k} \mathbf{s} = \text{Tr}\{\mathbf{B}_{q,k} \mathbf{s} \mathbf{s}^H\} = \text{Tr}\{\mathbf{B}_{q,k} \mathbf{Y}\}$ for $q = 1, \dots, K, k = 0, \dots, N-1$, such that $\mathbf{b}_q = [b_{q,0}, \dots, b_{q,N-1}]^T$. We have $i_{\text{dc}}(\{\mathbf{b}_q\}_{q=1}^K) = \sum_{q=1}^K \xi_q (\frac{1}{2}k_2 b_{q,0} + \mathbf{b}_q^H \mathbf{K}_0 \mathbf{b}_q)$. The problem becomes

$$\min_{t_2, \{\mathbf{b}_q\}_{q=1}^K} t_2 \quad (29a)$$

$$\text{s.t.} \quad \sum_{q=1}^K \xi_q \left(-\frac{1}{2}k_2 b_{q,0} - \mathbf{b}_q^H \mathbf{K}_0 \mathbf{b}_q \right) - t_2 \leq 0, \quad (29b)$$

$$\text{Tr}\{\mathbf{B}_{q,k} \mathbf{Y}\} = b_{q,k}, \forall q, k, \quad (29c)$$

$$\text{Tr}\{\mathbf{Y}\} \leq 2P, \quad (29d)$$

$$\text{rank}\{\mathbf{Y}\} = 1. \quad (29e)$$

Similar to the approach in Section III-A, we relax the rank constraint (29e) and use the SCA to solve it. Let $g(\mathbf{b}_q, \mathbf{b}_q^{(i-1)}) = 2\Re\{\mathbf{b}_q^{(i-1)H} \mathbf{K}_0 \mathbf{b}_q\} - \mathbf{b}_q^{(i-1)H} \mathbf{K}_0 \mathbf{b}_q^{(i-1)}$. We have $-\frac{1}{2}k_2 b_{q,0} - g(\mathbf{b}_q^{(i)}, \mathbf{b}_q^{(i)}) \leq -\frac{1}{2}k_2 b_{q,0} - g(\mathbf{b}_q^{(i)}, \mathbf{b}_q^{(i-1)}) \leq t_2$. Therefore, $-\frac{1}{2}k_2 b_{q,0} - g(\mathbf{b}_q, \mathbf{b}_q^{(i-1)}) \leq t_2$ can be seen as an upper bound convex constraint of initial non-convex constraint (29b). The problem can be rewritten as

$$\min_{t_2, \mathbf{b}_q, \mathbf{Y} \succeq 0} t_2 \quad (30a)$$

$$\text{s.t.} \quad -\frac{1}{2}k_2 b_{q,0} - g(\mathbf{b}_q, \mathbf{b}_q^{(i-1)}) - t_2 \leq 0, \quad (30b)$$

$$(29c) \text{ and } (29d) \quad (30c)$$

$$\mathbf{B}_q = \begin{pmatrix}
h_{q,1}^* h_{q,1} & h_{q,1}^* h_{q,2} & h_{q,1}^* h_{q,3} & h_{q,1}^* h_{q,4} & \cdots & h_{q,1}^* h_{q,N} \\
h_{q,2}^* h_{q,1} & h_{q,2}^* h_{q,2} & h_{q,2}^* h_{q,3} & h_{q,2}^* h_{q,4} & \cdots & \vdots \\
h_{q,3}^* h_{q,1} & h_{q,3}^* h_{q,2} & h_{q,3}^* h_{q,3} & h_{q,3}^* h_{q,4} & \cdots & \vdots \\
h_{q,4}^* h_{q,1} & h_{q,4}^* h_{q,2} & h_{q,4}^* h_{q,3} & h_{q,4}^* h_{q,4} & \cdots & \vdots \\
\vdots & \vdots & \vdots & \vdots & \ddots & \vdots \\
h_{q,N}^* h_{q,1} & \cdots & \cdots & \cdots & \cdots & h_{q,N}^* h_{q,N}
\end{pmatrix}$$

$k = 1$
 \downarrow

$k = 0 \rightarrow$
 $k = -1 \rightarrow$

Fig. 4. The definition of \mathbf{B}_q .

which can be written into a SDP as

$$\min_{\mathbf{Y}} \{ \text{Tr}\{\mathbf{K}_3 \mathbf{Y}\} : \text{Tr}\{\mathbf{Y}\} \leq 2P \} \quad (31)$$

where $\mathbf{K}_3 = \mathbf{J}_3 + \mathbf{J}_3^H$ is a Hermitian matrix and

$$\mathbf{J}_3 = \sum_{q=1}^K \xi_q \left(-\frac{k_2}{4} \mathbf{B}_{q,0} - \frac{3}{8} k_4 b_{q,0}^{(i-1)} \mathbf{B}_{q,0} - \frac{3}{4} k_4 \sum_{k=1}^{N-1} b_{q,k}^{(i-1)*} \mathbf{B}_{q,k} \right). \quad (32)$$

D. Alternating Optimization

For all the channel trails, we iteratively update the passive beamforming phases and waveform weights until convergence, which is shown in Algorithm 1 and Algorithm 2. In both algorithms, $[\mathbf{V}_{\mathbf{K}_3}]_{\min}$ refers to the eigenvector corresponding to the smallest eigenvalue which can be obtained via the eigenvalue decomposition (EVD) [41].

E. Convergence

Proposition 1: For any feasible initial points, Algorithm 1 can converge and provide a \mathbf{X}^* which satisfies the Karush-Kuhn-Tucker (KKT) conditions of problem (16), although there is no guarantee \mathbf{X}^* is rank-1.

Proof: See Appendix A. □

Proposition 2: If the \mathbf{X}^* in *Proposition 1* is rank-1, \mathbf{X}^* is also the local optimal solution of problem (13). Then, Algorithm 1 converges to a local optimal solution in (9).

Proof: See Appendix B. □

Proposition 3: For any feasible initial points, the passive beamforming vectors $\boldsymbol{\theta}^*$ generated by Algorithm 2 in problem (22) can guarantee the non-decreasing property of $\sum_{q=1}^K \xi_q i_{\text{dc},q}(\boldsymbol{\theta}^*)$. The Algorithm 2 can converge to a suboptimal point of (9).

Algorithm 1 MU FF-IRS WPT Algorithm

- 1: **Initialize:** $i=0$, $\{\mathbf{d}_q^{(0)}, \mathbf{b}_q^{(0)}, \mathbf{B}_q^{(0)}, \mathbf{D}_q^{(0)}\}_{q=1}^K, \mathbf{K}_1^{(0)}, \mathbf{K}_3^{(0)}, \Theta^{(0)}, \mathbf{y}^{(0)}$ and corresponding $t_2^{(0)}$;
 - 2: **Repeat**
 - 3: $i=i+1$;
 - 4: Update $\mathbf{K}_1^{(i)}$ and compute $\theta^{*(i)}$ using Gaussian randomization method in [44],
 $\Theta^{(i)*} = \text{diag}\{\theta^{*(i)}(1:L)\}$;
 - 5: Update $\mathbf{B}_{q,k}^{(i)}$ and $b_{q,k}^{(i)}, \forall q, k$;
 - 6: Update $\mathbf{K}_3^{(i)}$, get eigenvector $\mathbf{y}^* = \sqrt{2P}[\mathbf{V}_{\mathbf{K}_3}]_{\min}$; $\mathbf{Y}^* = \mathbf{y}^* \mathbf{y}^{*H}$;
 - 7: Update $\mathbf{Y}^{(i)} = \mathbf{Y}^*$. Then update $d_{q,k}^{(i)}, \mathbf{D}_{q,k}^{(i)}, \forall q, k$, compute $t_2^{(i)}$;
 - 8: **Until** $|t_2^{(i)} - t_2^{(i-1)}|/|t_2^{(i)}| \leq \varepsilon$ or $i \geq i_{\max}$
 - 9: $\mathbf{s}^* = \mathbf{y}^*$, output Θ^* .
-

Algorithm 2 MU FS-IRS WPT Algorithm

- 1: **Initialize:** $i=0$, $\{\mathbf{e}_q^{(0)}, \mathbf{b}_q^{(0)}, \mathbf{B}_q^{(0)}, \mathbf{E}_q^{(0)}\}_{q=1}^K, \mathbf{K}_2^{(0)}, \mathbf{K}_3^{(0)}, \{\Theta_n^{(0)}\}_{n=1}^N, \mathbf{y}^{(0)}$ and corresponding $t_2^{(0)}$;
 - 2: **Repeat**
 - 3: $i=i+1$;
 - 4: Update $\mathbf{K}_2^{(i)}$ and compute $\theta^{*(i)}$ using EWU and generate $\{\Theta_n^{(i)*}\}_{n=1}^N = \{\text{diag}\{\theta_n^{*(i)}(1:L)\}\}_{n=1}^N$;
 - 5: Update $\mathbf{B}_{q,k}^{(i)}$ and $b_{q,k}^{(i)}, \forall q, k$;
 - 6: Update $\mathbf{K}_3^{(i)}$, get eigenvector $\mathbf{y}^* = \sqrt{2P}[\mathbf{V}_{\mathbf{K}_3}]_{\min}$; $\mathbf{Y}^* = \mathbf{y}^* \mathbf{y}^{*H}$;
 - 7: Update $\mathbf{Y}^{(i)} = \mathbf{Y}^*$ and $e_{q,k}^{(i)}, \mathbf{E}_{q,k}^{(i)}, \forall q, k$ and compute $t_2^{(i)}$;
 - 8: **Until** $|t_2^{(i)} - t_2^{(i-1)}|/|t_2^{(i)}| \leq \varepsilon$ or $i \geq i_{\max}$
 - 9: $\mathbf{s}^* = \mathbf{y}^*$, output $\{\Theta_n^*\}_{n=1}^N$.
-

Proof: The SCA firstly ensures the non-decreasing property as $\theta^{*(i-1)}$ is also a feasible solution in iteration i . In the EWU method, (26) and (27) double guarantee the non-decreasing procedure by applying the complementary phasor of $\sum_{j=1, j \neq m} k_{m,j} \theta_j^*$ in (26). Due to the unit modulus constraint, the SCA based EWU strategy is upper bounded and finally converge. The Algorithm 2 is suboptimal due to the performance loss incurred by the EWU method. This performance loss is demonstrated in Fig. 16. \square

Proposition 4: For any feasible initial points, the waveform design subproblem in Section III-C can converge to the stationary points of problem (29) with $\sum_{q=1}^K \xi_q(i_{\text{dc},q}(\mathbf{s}^{*(i-1)})) \leq \sum_{q=1}^K \xi_q(i_{\text{dc},q}(\mathbf{s}^{*(i)}))$.

Proof: See [10] for detail. \square

F. Low Complexity Design for Single-user FS-IRS Scenario

In this section, we demonstrate an extra algorithm for SU FS-IRS for three reasons. First, Algorithm 2 can only provide suboptimal solutions due to the EWU strategy, but Algorithm 3 exhibits global optimal solutions. Second, Algorithm 3 further reduces the complexity compared with Algorithm 2 with $K = 1$ without the necessity of AO strategy. Third, Algorithm 2 can not boil down to Algorithm 3 when $K = 1$ since, in Algorithm 2, perfect alignment between the auxiliary channel and the direct channel may not be achieved, which incurs a performance loss compared with Algorithm 3. This performance loss is demonstrated in Fig. 16.

Because of the issues above, we demonstrate an efficient algorithm for SU FS-IRS by priorly determining the passive beamforming phases and waveform phases. For simpler notation, $h_{d,q,n}$ and $\mathbf{h}_{r,q,n}$ boil down to $h_{d,n}$ and $\mathbf{h}_{r,n}$ respectively. We denote $h_{d,n} = A_{d,n}e^{\phi_{d,n}}$, $h_{i,l+(n-1)L} = A_{i,l+(n-1)L}e^{\phi_{i,l+(n-1)L}}$ and $h_{r,l+(n-1)L} = A_{r,l+(n-1)L}e^{\phi_{r,l+(n-1)L}}$. Then, we denote the entries of $\mathbf{A}_{i,n}$ as $A_{i,l+(n-1)L}$ and the entries of $\mathbf{A}_{r,n}$ as $A_{r,l+(n-1)L}$ with $\mathbf{A}_{i,n} = [A_{i,1+(n-1)L}, \dots, A_{i,L+(n-1)L}]^T$ and $\mathbf{A}_{r,n} = [A_{r,1+(n-1)L}, \dots, A_{r,L+(n-1)L}]^T$, respectively. The passive beamforming and frequency domain power allocation for SU FS-IRS are sequentially demonstrated in the next sections.

1) *Passive Beamforming for Single-User FS-IRS*: Since FS-IRS is assumed to have an independent reflection for all frequencies with totally NL variables. When $K = 1$, each passive beamforming phase in FS-IRS can ideally align the auxiliary channel to the direct channel and the optimal passive beamforming phases and waveform phases have the values below

$$\gamma_n^* = -\phi_{d,n}, \forall n, \quad (33)$$

$$\psi_{l+(n-1)L}^* = -(\gamma_n^* + \phi_{i,l+(n-1)L} + \phi_{r,l+(n-1)L}), \forall n, l. \quad (34)$$

Remark 3: Recall that in Section III-C, we directly optimize the waveform weight \mathbf{s}_n which consists of the amplitude w_n and phase γ_n . In contrast, due to the prior determination of γ_n , the joint passive beamforming and waveform design in SU FS-IRS is essentially the frequency domain power allocation at different frequencies, i.e. w_n , and naturally exhibits lower complexity than SCA based AO strategy in MU FS-IRS.

2) *Frequency Domain Power Allocation for Single-User FS-IRS*: Due to the ideal alignment of composite channel in SU FS-IRS, we denote the corresponding composite channel $A_n = A_{d,n} + \mathbf{A}_{r,n}\mathbf{A}_{i,n}$ which

is collected into $\mathbf{A} = [A_1, \dots, A_N]^T$ and group w_n into the power allocation vector $\mathbf{p} = [w_1, w_2, \dots, w_N]^T$.

Objective function (8) is transformed to

$$i_{\text{dc}}(\mathbf{p}) = \frac{1}{2}k_2 \sum_{n=1}^N w_n^2 A_n^2 + \frac{3}{8}k_4 \sum_{\substack{n_1, n_2, n_3, n_4 \\ n_1 + n_3 = n_2 + n_4}} w_{n_1} A_{n_1} A_{n_2} w_{n_2} w_{n_3} A_{n_3} A_{n_4} w_{n_4}. \quad (35)$$

We can formulate (35) into a more compact form by introducing N -by- N matrices \mathbf{B} and \mathbf{B}_k where $\mathbf{B} = \mathbf{A}\mathbf{A}^T$. $k \in \{1, \dots, N-1\}$ denotes the index of the k th diagonal above the main diagonal (with the index $k=0$) of the matrix \mathbf{B} . $k \in \{-(N-1), \dots, -1\}$ denotes the index of the $|k|$ th diagonal below the main diagonal. \mathbf{B}_k is obtained by retaining the k th diagonal of \mathbf{B} with other entries as zeros. The compact form of (35) can be expressed as

$$i_{\text{dc}}(\mathbf{p}) = \frac{1}{2}k_2 \mathbf{p}^H \mathbf{B}_0 \mathbf{p} + \frac{3}{8}k_4 \mathbf{p}^H \mathbf{B}_0 \mathbf{p} (\mathbf{p}^H \mathbf{B}_0 \mathbf{p})^H + \frac{3}{4}k_4 \sum_{k=1}^{N-1} \mathbf{p}^H \mathbf{B}_k \mathbf{p} (\mathbf{p}^H \mathbf{B}_k \mathbf{p})^H. \quad (36)$$

To maximize the output DC current under the power constraint at transmitter, the problem can be formulated as

$$\max_{\mathbf{p}} \{i_{\text{dc}}(\mathbf{p}) : \|\mathbf{p}\|^2 \leq 2P\}. \quad (37)$$

Similar to that in Section III-C, we introduce a rank-1 positive semidefinite matrix variable $\mathbf{P} = \mathbf{p}\mathbf{p}^H$ to linearize the problem with $b_k = \mathbf{p}^H \mathbf{B}_k \mathbf{p} = \text{Tr}\{\mathbf{B}_k \mathbf{P}\}$. Then, denote $\mathbf{b} = [b_0, b_1, \dots, b_{N-1}]^T$. Finally, we have $i_{\text{dc}}(\mathbf{b}) = \frac{1}{2}k_2 b_0 + \frac{3}{8}k_4 b_0 b_0^* + \frac{3}{4}k_4 \sum_{k=1}^{N-1} b_k b_k^* = \frac{1}{2}k_2 b_0 + \mathbf{b}^H \mathbf{K}_0 \mathbf{b}$. The problem (37) can be equivalently written as

$$\min_{t_3, \mathbf{b}, \mathbf{P} \succeq 0} t_3 \quad (38a)$$

$$\text{s.t.} \quad -i_{\text{dc}}(\mathbf{b}) - t_3 \leq 0, \quad (38b)$$

$$\text{Tr}\{\mathbf{B}_k \mathbf{P}\} = b_k, \forall k, \quad (38c)$$

$$\text{Tr}\{\mathbf{P}\} \leq 2P, \quad (38d)$$

$$\text{rank}\{\mathbf{P}\} = 1. \quad (38e)$$

After the relaxation of rank constraint and SCA approach, the compact form of problem (37) can be formulated as

$$\min_{\mathbf{P} \succeq 0} \{\text{Tr}\{\mathbf{K}_4 \mathbf{P}\} : \text{Tr}\{\mathbf{P}\} \leq 2P\} \quad (39)$$

where $\mathbf{K}_4 = \mathbf{J}_4 + \mathbf{J}_4^H$ is a Hermitian matrix and $\mathbf{J}_4 = -\frac{k_2}{4} \mathbf{B}_0 - \frac{3}{8}k_4 b_0^{(i-1)} \mathbf{B}_0 - \frac{3}{4}k_4 \sum_{k=1}^{N-1} b_k^{(i-1)*} \mathbf{B}_k$. The whole procedure is summarized in Algorithm 3.

Remark 4: According to [10], problem (39) has a rank-1 global optimal solution $\mathbf{P}^* = \mathbf{p}^* \mathbf{p}^{*H}$ with $\mathbf{p}^* = \sqrt{2P} [\mathbf{V}_{\mathbf{K}_4}]_{\min}$, which is different from that in generalized MU scenario as the EWU based strategy

Algorithm 3 SU FS-IRS WPT Algorithm

- 1: **Initialize:** $i=0$ and $\mathbf{b}^{(0)}$, $\mathbf{p}^{(0)}$ and $t_3^{(0)}$;
 - 2: **Repeat**
 - 3: $i=i+1$
 - 4: Compute $\mathbf{K}_4 = \mathbf{J}_4 + \mathbf{J}_4^H$, get eigenvector $\mathbf{p}^* = \sqrt{2P}[\mathbf{V}_{\mathbf{K}_4}]_{\min}$; $\mathbf{P}^* = \mathbf{p}^* \mathbf{p}^{*H}$;
 - 5: Update $\mathbf{P}^{(i)} = \mathbf{P}^*$; Update $b_k^{(i)} = \text{Tr}\{\mathbf{B}_k \mathbf{P}^{(i)}\}, \forall k$;
 - 6: Update $t_3^{(i)}$;
 - 7: **Until** $|t_3^{(i)} - t_3^{(i-1)}|/|t_3^{(i)}| \leq \varepsilon$ or $i \geq i_{\max}$
 - 8: $s_n^* = [\mathbf{p}^*]_{n,1} \cdot h_n^* / |h_n|, \forall n$.
-

can only provide suboptimal solutions. In each iteration, the rank-1 global optimal solution not only guarantees to demonstrate convergence to the stationary points of the relaxed problem (39) but also the original problem (38).

G. Discussion on Large Scale Scenario of SU FS-IRS

This subsection proposes a brief analysis of the performance of SU FS-IRS in the limit of a large number of REs L and frequencies N . We assume that all the channels are uncorrelated. Given the large scale fading for $h_{d,n}, h_{i,l+(n-1)L}$ and $h_{r,l+(n-1)L}$ as $\Lambda_d^{1/2}, \Lambda_i^{1/2}$ and $\Lambda_r^{1/2}$, respectively, under the perfect alignment in SU FS-IRS, we have

$$\mathcal{E}\{|h_n|\} = \mathcal{E}\left\{\sqrt{|h_{d,n} + \sum_{l=1}^L h_{r,l+(n-1)L} \theta_{l+(n-1)L} h_{i,l+(n-1)L}|^2}\right\} \stackrel{L \rightarrow \infty}{\approx} \sqrt{\Lambda_d + \Lambda_i \Lambda_r L^2}. \quad (40)$$

According to [10], with uniform power allocation across frequencies, we can approximate the output current as

$$i_{dc} \stackrel{N \rightarrow \infty}{\approx} k_2 P (\Lambda_d + \Lambda_i \Lambda_r L^2) + \frac{3}{2} k_4 P^2 (\Lambda_d + \Lambda_i \Lambda_r L^2)^2 + 3k_4 P^2 (\Lambda_d + \Lambda_i \Lambda_r L^2)^2 N. \quad (41)$$

Therefore, if the number of L is large, the output current will scale up with the square number of L^2 (i.e. L^4) which is shown in (41) and validated in Fig. 7. This is due to the nonlinearity of the rectenna model which is truncated to $n_0=4$. In addition, if N is large enough, the output DC current linearly scales with N which is validated in Section IV⁵. This is inline with the scaling law in [7].

⁵Based on the rectenna model in Section II-D, increasing the number of subcarriers improves the harvested DC power as long as the EH does not operate in the saturation region. In a practical prototype of No-IRS WPT, due to the Peak-to-Average Power Ratio (PAPR) limits of the transmitter, 16 is a good number which was experimentally observed in [11], [19].

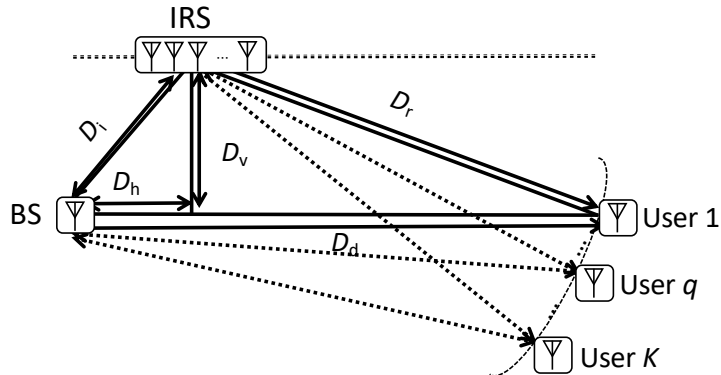


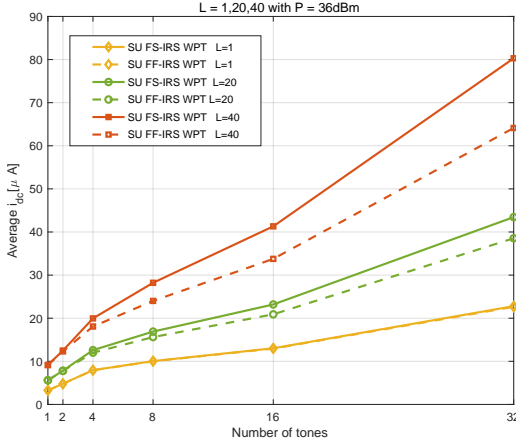
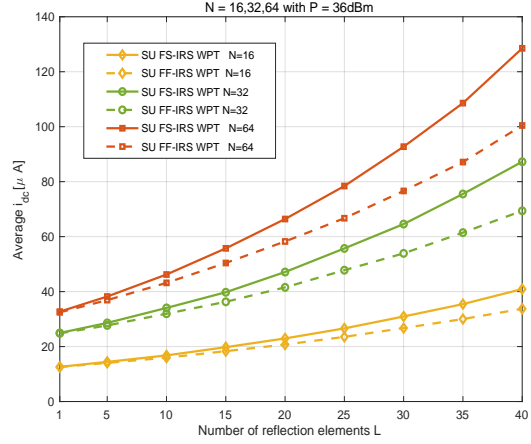
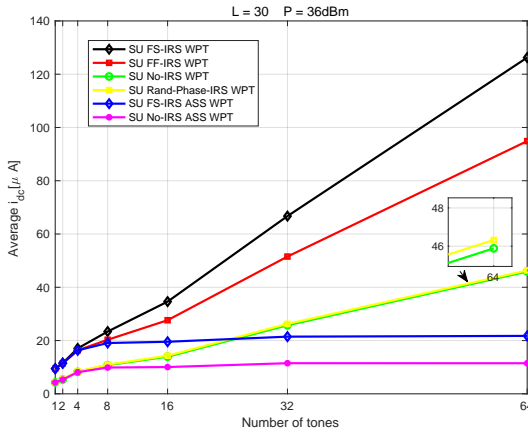
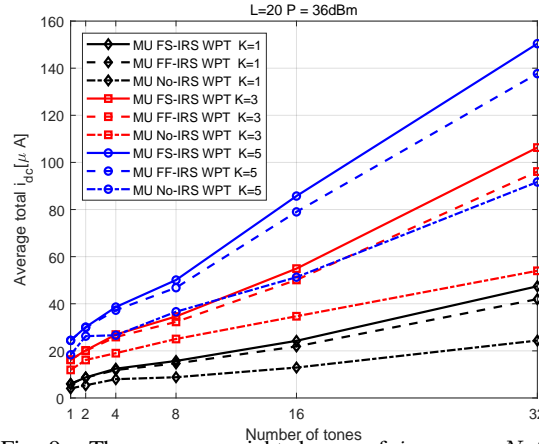
Fig. 5. Simulation layout.

IV. NUMERICAL RESULT

We now evaluate the performance in a typical open space WiFi-like environment under a transmit power constraint of 36 dBm at a central frequency of 5.18 GHz with signal bandwidth being fixed to 10MHz as a baseline unless otherwise stated. A uniform linear array (ULA) at the IRS with half wavelength spacing are considered in our model. The pathloss model is shown below

$$T_j(D_j) = r_0 \left(\frac{D_j}{d_0} \right)^{-\nu_j} \quad (42)$$

where r_0 is the large scale fading parameter at reference distance $d_0 = 1\text{m}$ with D_j and ν_j referring to the distance and pathloss exponent, respectively, for $j \in \{d, i, r\}$. All the channels are modeled as Rayleigh fading NLOS channels with the path loss exponents and power delay profiles coming from model D in [48]. 18 taps are modeled as i.i.d CSCG random variables to generate uncorrelated frequency-selective fading channels. According to Fig. 5, $D_i = \sqrt{D_h^2 + D_v^2}$ and $D_r = \sqrt{D_v^2 + (D_d - D_h)^2}$ with D_h and D_v referring horizontal distance and vertical distance, respectively. Parameters are assigned as $D_v = 2\text{m}$, $D_h = 2\text{m}$ and $D_d = 15\text{m}$ as a baseline unless specified later. Without loss of generality, the reference path loss for all users is set as -35dB at 1m. For all the numerical figures, SU FS-IRS and MU FS-IRS simulation results come from Algorithm 3 and 2, respectively. Both SU FF-IRS and MU FF-IRS results are generated from Algorithm 1 for choices of $K = 1$ and $K > 1$, respectively. The sufficient small tolerance of stopping threshold in all algorithms is set as 10^{-4} and each point in the following figures is acquired via averaging over 1000 independent realizations. The number of candidates for Gaussian randomization in Algorithm 1 is 1000.

Fig. 6. Average i_{dc} versus N for $L=1,20,40$.Fig. 7. Average i_{dc} versus L for $N=16,32,64$.Fig. 8. Average i_{dc} versus N .Fig. 9. The average weighted sum of i_{dc} versus N for $K=1,3,5$ and $L=20$.

A. Single-User

We first characterize the average output DC current versus the number of sinewaves N with different number of passive reflecting elements L in Fig. 6 and 7. A *first* observation is that the output DC current of both SU FS-IRS and SU FF-IRS increases with the number of sinewaves N and SU FS-IRS can be seen as a performance upper bound of the corresponding SU FF-IRS scenario. When $N=1$, SU FF-IRS displays exactly the same current with SU FS-IRS. A *second* observation is that the output current approximately scales up with the L^4 . This is, thus, envisioned to revolutionize large-scale design since a large L can compensate for the small number of transmit antennas. A *third* observation is that the performance gap between SU FS-IRS and SU FF-IRS is gradually increased with N and SU FS-IRS observes a gain of 28% over SU

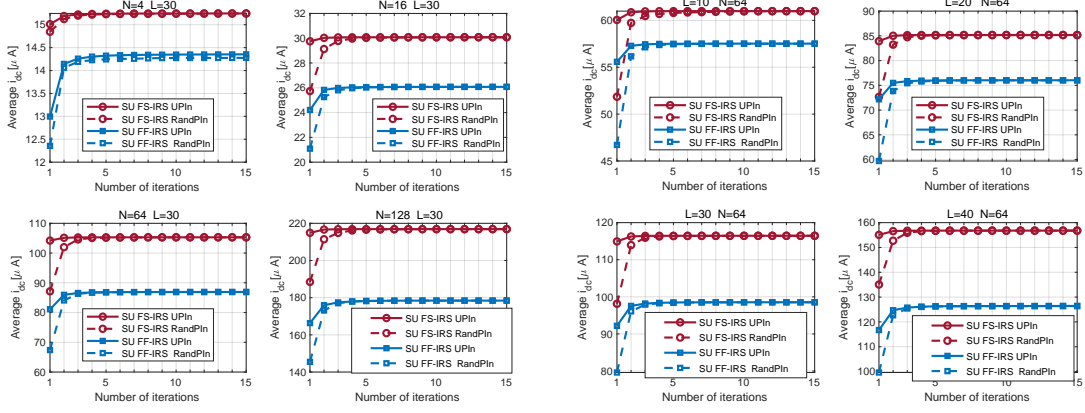


Fig. 10. Average i_{dc} versus number of iterations for Fig. 11. Average i_{dc} versus number of iterations for $N=4,16,64,128$ and $L=30$. $L=10,20,30,40$ and $N=64$.

FF-IRS when $N=64, L=40$. The reason behind such a phenomenon is that, in SU FS-IRS, ideal passive beamforming phases can always align the composite channel. While, in SU FF-IRS, more performance loss is incurred by the misalignment between the auxiliary channel and the direct channel with larger N .

An overview of average output DC current versus the number of sinewaves N is clearly exhibited in Fig. 8. SU FS-IRS, SU FF-IRS and SU Rand-Phase-IRS WPT refer to nonlinear-based rectenna model with different IRS scenarios. SU No-IRS WPT refers to conventional WPT designs in [7]. SU FS-IRS ASS and SU No-IRS ASS denote the ASS strategy based linear-based rectenna model (a truncating order of 2) [7][10] with FS-IRS and without IRS, respectively⁶. We make the following observations.

First, if taking SU FS-IRS ASS WPT as a benchmark, SU FS-IRS and SU FF-IRS can exceed the benchmark on around 550% and 400%, respectively, when $N=64$. This result strongly embodies the superiority of nonlinear based rectenna model over ASS based linear rectenna model, showing that the output DC current can be effectively boosted by leveraging the gain from rectenna nonlinearity for both FS-IRS and FF-IRS scenarios.

Second, both SU FS-IRS and SU FF-IRS observe a great performance gain over No-IRS scenario on around 195% and 155%, respectively, when $N=64, L=30$. An explanation is that both of them consolidate the composite channel strength with passive beamforming phases manipulation. Furthermore,

⁶The output current for user q under a linear based model (a truncating order of 2) is given as $i_{dc,q}(\mathbf{s}, \{\Theta_n\}_{n=1}^N) = \frac{1}{2}k_2 \sum_{n=1}^N \mathfrak{e}_n^* h_{q,n}^* h_{q,n} s_n$. Compared with (8), the maximization of output current can be efficiently solved by allocating all the power to the strongest frequency-selective channel which leads to the ASS strategy in Fig. 8.

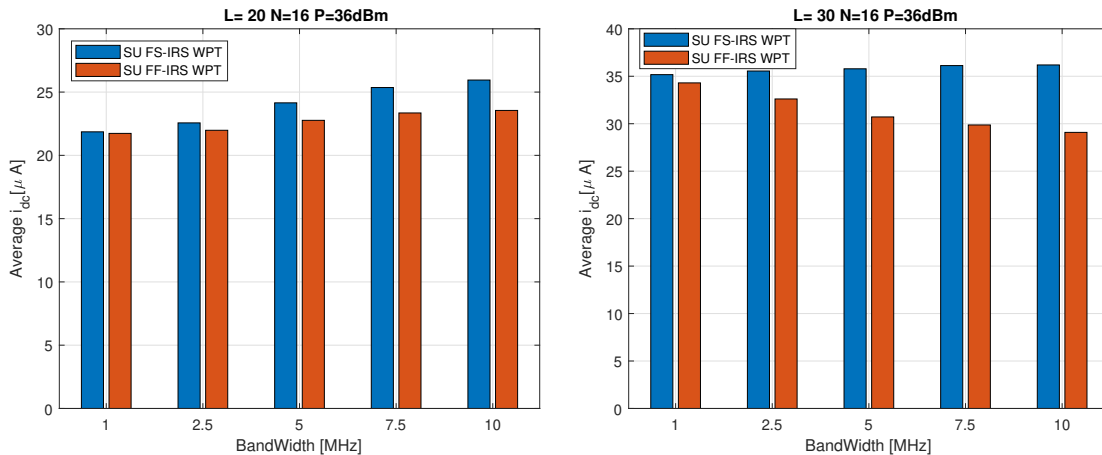


Fig. 12. Average i_{dc} versus bandwidth for $L=20$ and $N=16$. Fig. 13. Average i_{dc} versus bandwidth for $L=30$ and $N=16$.

it is worth pointing out that although SU FF-IRS is outperformed by SU FS-IRS, it still achieves non-negligible performance improvement over No-IRS conventional WPT waveform designs in [7][10].

Third, SU Rand-Phase-IRS displays a similar output current with No-IRS scenario which emphasizes the significance of the passive beamforming design. Without the optimization of the passive beamforming phases, the signal attenuation can not be effectively alleviated by IRS as different cascaded channels superpose randomly instead of constructively.

B. Convergence Analysis

Fig. 10 and 11 illustrate the average output DC current versus the number of iterations for different initialization strategies. The initial passive beamforming phases are randomly chosen in $[0, 2\pi)$. The frequency domain power allocation strategies are "UPIn" and "RandPIn" referring uniform power allocation and random power allocation, respectively. First, "UPIn" exhibits a faster convergence than "RandPIn", which suggests the potential benefits of uniform power allocation in large scale SU FS-IRS and SU FF-IRS WPT. Second, both "UPIn" and "RandPIn" converge to nearly the same objective function values. An explanation is that considering the non-convexity in problem (13), various initial points may lead to different solutions in Algorithm 1. However, solution \mathbf{X}^* is demonstrated to be a rank-1 solution in all tested channels and strongly reduces the performance loss incurred by Gaussian randomization method, which contributes to the insensitivity of initial power allocation and initial passive beamforming phases.

C. Bandwidth

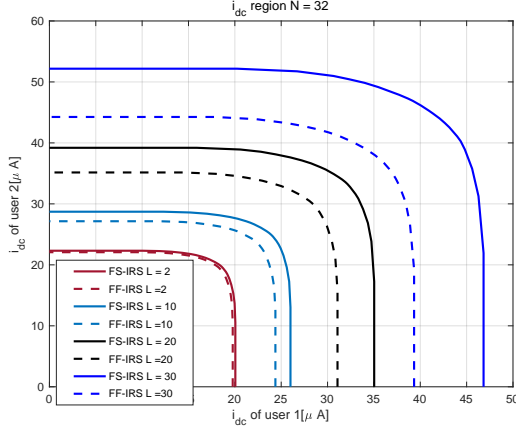
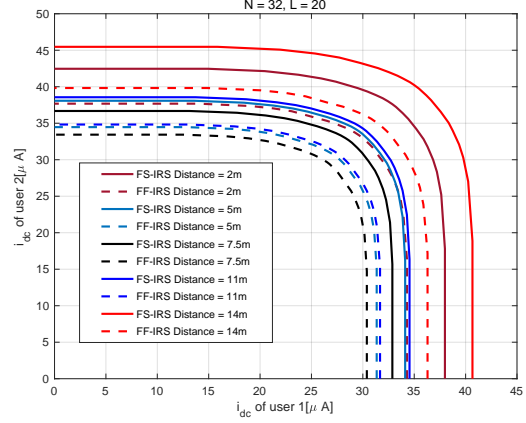
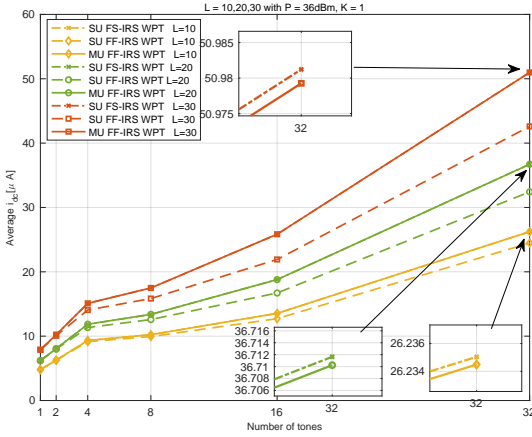
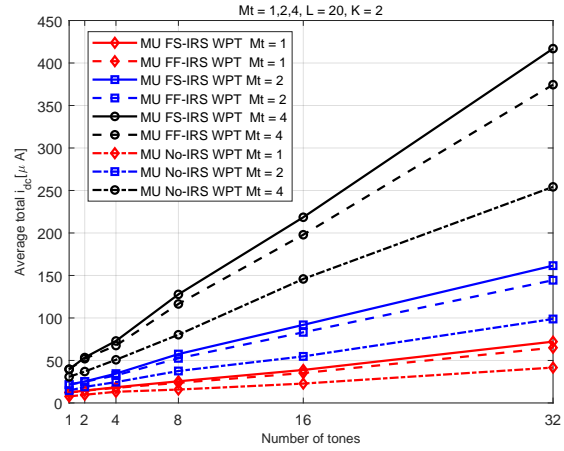
Fig. 12 and Fig. 13 explores the sensitivity of i_{dc} to different bandwidths from 1MHz to 10 MHz for $L=20$ and $L=30$, respectively. A *first* observation is that the gap between SU FS-IRS and SU FF-IRS in both figures increases with the bandwidth which emphasizes the superiority of SU FS-IRS over SU FF-IRS on output DC current by favouring the strongest sinewaves more efficiently. A *second* observation is that the output DC current of SU FS-IRS increases slowly with the bandwidth and the opposite behavior is observed in SU FF-IRS. An explanation is that, when $L=20$, both SU FS-IRS and SU FF-IRS benefit from increasing frequency selectivity which contributes to an ascending trend. However, when $L=30$, the misalignment of composite channel in SU FF-IRS becomes more pronounced with increasing bandwidth, which renders a descending trend.

To conclude, SU FF-IRS is not equally suitable for broadband and narrowband WPT, namely, SU FF-IRS works well in narrowband systems but incurs some loss in a higher bandwidth transmission. In contrast, SU FS-IRS offers a promising gain over SU FF-IRS by flexibly favouring passive beamforming phases in a frequency-selective design but also incurs a higher hardware complexity.

D. Multi-User

The average weighted sum current versus the number of sinewaves N for different number of users K is shown in Fig. 9. The weight ξ_q for each user is 1. It is first observed that MU FF-IRS incurs a performance loss compared with MU FS-IRS and the performance gap increases with K . This is expected since MU FF-IRS suffers more misalignment on different user's composite channels than MU FS-IRS by constraining the passive beamforming phases to be the same across frequencies, which stresses the natural benefits of developing more flexible IRS hardware to enable adaptive frequency-selective passive beamforming phase shifts.

Fig. 14 draws a useful insight into the average i_{dc} region (obtained by solving problem (9) with varying weights (ξ_1, ξ_2)) versus the number of reflecting elements L in a two user system. It is observed that the current regions of two IRS strategies gradually increase with L . This is intuitive since both FS-IRS and FF-IRS can compensate the distance-dependent path loss by strengthening the composite channel of each user. Due to the additional design flexibility in the frequency domain, FS-IRS provides better channel alignment and it enlarges the region more than FF-IRS. This characteristic highlights the advancement of IRS in frequency-selective design. To further unveil the impact of the IRS position, based on the same user weight pairs as Fig. 14, Fig 15 demonstrates the current region versus the horizontal distances, i.e. D_h , with $D_v = 2\text{m}$ as a constant. One can observe that the regions are effectively enlarged when IRS is

Fig. 14. i_{dc} region versus L for $N = 32$.Fig. 15. i_{dc} region versus D_h for $N = 32$ and $L = 20$.Fig. 16. Average i_{dc} versus N for $L = 10, 20, 30$ and $K = 1$.Fig. 17. Average weighted sum i_{dc} versus N for $L = 20$, number of transmit antennas $M_t = 1, 2, 4$ and $K = 2$.

installed either near the BS or near the users. The comparison between Algorithm 2 and Algorithm 3 with $K = 1$ is demonstrated in Fig. 16. Due to suboptimal operation of EWU strategy, Algorithm 2 exhibited a slightly loss in contrast with Algorithm 3. However, this loss is small enough to be negligible (less than 0.1%) which, instead, reveals the generality and superiority of Algorithm 2. The impact of joint waveform, active and passive beamforming is demonstrated in Fig. 17 which explores the average weighted sum current versus the number of sinewaves N for different number of transmit antenna M_t . It is observed that the weighted sum output current of both MU FF-IRS and MU FS-IRS approximately scale up with the square number of M_t . Compared with single-antenna scenario in Fig. 7, active beamforming is envisioned

to further boost the output DC power.

E. Discrete-Phase

To extend to the discrete-phase IRS problem, one widely used strategy is to relax the discrete IRS problems to their continuous counterparts and obtain quantized phases $\tilde{\psi}_{l+(n-1)L} \forall n, l$ in phase set \mathcal{S} by mapping the continuous values to their closest discrete value in \mathcal{S} with mapping function \mathcal{F} [46] which is given as

$$\tilde{\psi}_{l+(n-1)L} = \mathcal{F}(\psi_{l+(n-1)L}), \forall l, n, \quad (43)$$

$$\tilde{\psi}_{l+(n-1)L} \in \mathcal{S}, \forall l, n, \quad (44)$$

where $\mathcal{S} = \{0, \Delta\psi, \dots, \Delta\psi(2^M - 1)\}$ denotes the equally spaced phase set with $\Delta\psi = 2\pi/2^M$ and M denotes the resolution bits. Leveraging this discrete-phase strategy in [46], Fig. 18 and 19 are plotted for single-user and multi-user conditions, respectively.

Fig. 18 demonstrates the average output DC current versus L with $N = 32$ and quantization scheme $M = 1, 2, 3$ bits for single-user scenario. *First*, it is observed that the i_{dc} for both SU FF-IRS and SU FS-IRS can be greatly improved compared with No-IRS condition even with 1-bit phase shifter. *Second*, one can observe that the performance loss incurred by discrete phases decreases with an increasing number of resolution bits. This is intuitive since a larger number of bits enables a better alignment between channels. Under the same quantization scheme, right figure illustrates the weighted sum current versus N with $L = 20$ and $K = 3$. The performance gain of 1-bit resolution current over No-IRS benchmark increases with the number of subcarriers N , which suggests the effectiveness of deploying discrete-phase IRS in wideband WPT. Moreover, the performance loss incurred by discrete-IRS is low with 3-bit resolution phase shifters, which confirms that directly quantizing the optimized continuous RE phases can achieve near-optimal performance in multi-user scenario.

V. CONCLUSION AND FUTURE WORK

In this paper, we investigated the joint waveform and passive beamforming design for IRS-aided wireless power transfer for both single-user and multi-user deployments. Two different formulations were developed based on a FS-IRS and FF-IRS. An optimization framework based on AO and SCA was studied and demonstrated robustness with fast convergence. Numerical results confirmed the inefficiency of linear based model and highlight the fact that even FF-IRS-aided WPT can outperform conventional

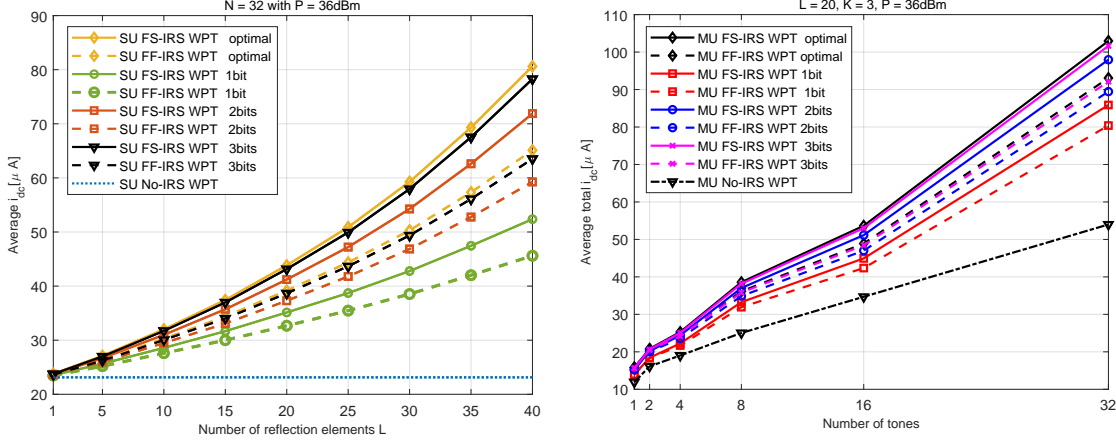


Fig. 18. Average i_{dc} versus L for $N = 32$ and resolution bits $M = 1,2,3$. Fig. 19. Average weighted sum i_{dc} versus N for $M = 1,2,3$, $L = 20$ and $K = 3$.

WPT designs with IRS passive beamforming gain. Furthermore, FS-IRS acted as a canonical upper bound for broadband system while FF-IRS was suitable for narrowband transmission. Moreover, for WPT system, the assistance of IRS not only expanded the operation range for SU conditions, but also enlarged the output DC current region in MU scenarios. In addition, this AO framework can be directly extended to multi-antenna scenario to explore the transmit beamforming gain. Last but not least, a near-optimal result can be achieved by leveraging low-resolution discrete-phase IRS for both SU and MU scenarios.

Several important issues are not addressed in our paper: first, how to formulate the waveform design and passive beamforming for MU minimum i_{dc} maximization problem (Max-Min problem) [10]; second, how to involve more advanced group/fully connected IRS into WPT system [27]; third, how to design waveform, transmit active beamforming, receive combining and passive beamforming in a multi-user MIMO WPT scenario [18]; fourth, how to relax the constraint on assumptions of the EH model (ideal low pass filter with infinite RC constant) and explore this more accurate and complicated rectenna model by using machine learning techniques [49].

APPENDIX A

PROOF OF PROPOSITION 1

We first prove the convergence of problem (16). $f(\mathbf{d}_q)$ and $f(\mathbf{d}_q, \mathbf{d}_q^{(i-1)})$ are demonstrated below

$$f(\mathbf{d}_q) = \mathbf{d}_q^H \mathbf{K}_0 \mathbf{d}_q, \quad (45)$$

$$f(\mathbf{d}_q, \mathbf{d}_q^{(i-1)}) = 2\Re\{\mathbf{d}_q^{(i-1)H} \mathbf{K}_0 \mathbf{d}_q\} - \mathbf{d}_q^{(i-1)H} \mathbf{K}_0 \mathbf{d}_q^{(i-1)}. \quad (46)$$

According to [41], it can be checked that $f(\mathbf{d}_q^{(i)}, \mathbf{d}_q^{(i)}) = f(\mathbf{d}_q^{(i)})$. Since the solution vector $\mathbf{d}_q^{(i-1)}$ is a feasible solution in iteration $i-1$, by using the inequality in Taylor expansion, we have $f(\mathbf{d}_q^{(i)}) \geq f(\mathbf{d}_q^{(i)}, \mathbf{d}_q^{(i-1)})$ which proves that $f(\mathbf{d}_q^{(i)})$ is monotonically increasing. Additionally, problem (16) must have an upper bound due to the unit modulus constraint (16b). Hence, problem (16) is guaranteed to converge.

Now, we prove that the convergent solution is a KKT solution of problem (13). (16a) and (16b) are convex problems with respect to \mathbf{X} and satisfies the Slater's condition [50], the dual gap is zero and strong duality hold. The optimal solution \mathbf{X}^* can be get by figuring out its dual problem. The corresponding Lagrange function of problem (16) is

$$\mathcal{L}(\mathbf{X}, \boldsymbol{\tau}) = \text{Tr}\{\mathbf{K}_1 \mathbf{X}\} + \sum_{l'=1}^{L+1} \tau_{l'} (\mathbf{X}_{l', l'} - 1) + \boldsymbol{\Upsilon} \mathbf{X} \quad (47)$$

where $\boldsymbol{\tau} = \{\tau_1, \tau_2, \dots, \tau_{L+1}\}$ and $\boldsymbol{\Upsilon}$ denote the vector and matrix dual variables of (16b) and (16c). There must be a $\boldsymbol{\tau}^* = \{\tau_1^*, \tau_2^*, \dots, \tau_{L+1}^*\}$ and $\boldsymbol{\Upsilon}^*$ for guaranteeing that the corresponding KKT conditions are satisfied

$$\nabla_{\mathbf{X}^*} \mathcal{L}(\mathbf{X}, \boldsymbol{\tau})|_{\mathbf{X}=\mathbf{X}^*} = \mathbf{0} \quad (48)$$

$$\tau_{l'}^* (\mathbf{X}_{l', l'}^* - 1) = 0, \forall l' \quad (49)$$

$$\boldsymbol{\Upsilon}^* \mathbf{X}^* = \mathbf{0} \quad (50)$$

The KKT conditions of problem (16) exactly consist of (48), (49) and (50). Hence, *Proposition 1* holds.

APPENDIX B

PROOF OF PROPOSITION 2

Due to the equivalence between problem (15) and problem (16), (48)-(50) are also the KKT conditions of problem (15). From (14), we have

$$\nabla_{\mathbf{d}_q = \mathbf{d}_q^*} f(\mathbf{d}_q)|_{\mathbf{d}_q = \mathbf{d}_q^*} = \nabla_{\mathbf{d}_q = \mathbf{d}_q^*} f(\mathbf{d}_q, \mathbf{d}_q^{(i-1)})|_{\mathbf{d}_q = \mathbf{d}_q^*} \quad (51)$$

Since problem (13b) and problem (15b) exactly contain $f(\mathbf{d}_q)$ and $f(\mathbf{d}_q, \mathbf{d}_q^{(i-1)})$ at iteration i , respectively, except some constants, upon denoting the (13b) as $p(\mathbf{d}_q) = \sum_{q=1}^K \xi_q(-\frac{1}{2}k_2 d_{q,0} - f(\mathbf{d}_q))$ and (15b) as $p(\mathbf{d}_q, \mathbf{d}_q^{(i-1)}) = \sum_{q=1}^K \xi_q(-\frac{1}{2}k_2 d_{q,0} - f(\mathbf{d}_q, \mathbf{d}_q^{(i-1)}))$, we arrive at

$$\nabla_{\mathbf{d}_q=\mathbf{d}_q^*} p(\mathbf{d}_q)|_{\mathbf{d}_q=\mathbf{d}_q^*} = \nabla_{\mathbf{d}_q=\mathbf{d}_q^*} p(\mathbf{d}_q, \mathbf{d}_q^{(i-1)})|_{\mathbf{d}_q=\mathbf{d}_q^*}. \quad (52)$$

According to (51) and relation between $p(\mathbf{d}_q)$ and $p(\mathbf{d}_q, \mathbf{d}_q^{(i-1)})$, KKT conditions of problem (13) exactly consist of (48), (49) and (50) and \mathbf{X}^* is also a local optimal solution for problem (13). Combining the proof above and *Proposition 4*, a local optimal solution for passive beamforming subproblem and a global optimal solution for waveform design subproblem can be obtained. Hence, the AO Algorithm 1 converges to a local optimal solution in original problem (9) and *Proposition 2* holds.

REFERENCES

- [1] B. Clerckx, A. Costanzo, A. Georgiadis, and N. Borges Carvalho, "Toward 1G Mobile Power Networks: RF, Signal, and System Designs to Make Smart Objects Autonomous," *IEEE Microwave Magazine*, vol. 19, no. 6, pp. 69–82, 2018.
- [2] B. Clerckx, R. Zhang, R. Schober, D. W. K. Ng, D. I. Kim, and H. V. Poor, "Fundamentals of wireless information and power transfer: From RF energy harvester models to signal and system designs," *IEEE Journal on Selected Areas in Communications*, vol. 37, no. 1, pp. 4–33, 2018.
- [3] C. R. Valenta and G. D. Durgin, "Harvesting wireless power: Survey of energy-harvester conversion efficiency in far-field, wireless power transfer systems," *IEEE Microwave Magazine*, vol. 15, no. 4, pp. 108–120, 2014.
- [4] S. Shen, C. Chiu, and R. D. Murch, "A Dual-Port Triple-Band L-Probe Microstrip Patch Rectenna for Ambient RF Energy Harvesting," *IEEE Antennas and Wireless Propagation Letters*, vol. 16, pp. 3071–3074, 2017.
- [5] —, "Multiport Pixel Rectenna for Ambient RF Energy Harvesting," *IEEE Transactions on Antennas and Propagation*, vol. 66, no. 2, pp. 644–656, 2018.
- [6] Y. Zeng, B. Clerckx, and R. Zhang, "Communications and Signals Design for Wireless Power Transmission," *IEEE Transactions on Communications*, vol. 65, no. 5, pp. 2264–2290, 2017.
- [7] B. Clerckx and E. Bayguzina, "Waveform design for wireless power transfer," *IEEE Transactions on Signal Processing*, vol. 64, no. 23, pp. 6313–6328, 2016.
- [8] A. Collado and A. Georgiadis, "Optimal waveforms for efficient wireless power transmission," *IEEE Microwave and Wireless Components Letters*, vol. 24, no. 5, pp. 354–356, 2014.
- [9] B. Clerckx and E. Bayguzina, "Low-complexity adaptive multisine waveform design for wireless power transfer," *IEEE Antennas and Wireless Propagation Letters*, vol. 16, pp. 2207–2210, 2017.
- [10] Y. Huang and B. Clerckx, "Large-scale multiantenna multisine wireless power transfer," *IEEE Transactions on Signal Processing*, vol. 65, no. 21, pp. 5812–5827, 2017.
- [11] J. Kim, B. Clerckx, and P. D. Mitcheson, "Signal and System Design for Wireless Power Transfer : Prototype, Experiment and Validation," *IEEE Transactions on Wireless Communications*, pp. 1–1, 2020.
- [12] Y. Huang and B. Clerckx, "Waveform design for wireless power transfer with limited feedback," *IEEE Transactions on Wireless Communications*, vol. 17, no. 1, pp. 415–429, 2017.
- [13] S. Shen, J. Kim, and B. Clerckx, "Closed-loop wireless power transfer with adaptive waveform and beamforming: Design, prototype, and experiment," *arXiv preprint arXiv:2106.03519*, 2021.

- [14] J. Xu and R. Zhang, "Energy beamforming with one-bit feedback," *IEEE Transactions on Signal Processing*, vol. 62, no. 20, pp. 5370–5381, 2014.
- [15] M.-L. Ku, Y. Han, B. Wang, and K. R. Liu, "Joint power waveforming and beamforming for wireless power transfer," *IEEE Transactions on Signal Processing*, vol. 65, no. 24, pp. 6409–6422, 2017.
- [16] D. Masotti, A. Costanzo, M. Del Prete, and V. Rizzoli, "Time-modulation of linear arrays for real-time reconfigurable wireless power transmission," *IEEE Transactions on Microwave Theory and Techniques*, vol. 64, no. 2, pp. 331–342, 2016.
- [17] S. Shen and B. Clerckx, "Beamforming Optimization for MIMO Wireless Power Transfer with Nonlinear Energy Harvesting: RF Combining versus DC Combining," *IEEE Transactions on Wireless Communications*, pp. 1–1, 2020.
- [18] S. Shen and B. Clerckx, "Joint Waveform and Beamforming Optimization for MIMO Wireless Power Transfer," 2020.
- [19] J. Kim and B. Clerckx, "Range Expansion for Wireless Power Transfer: A Joint Beamforming and Waveform Architecture," 2020.
- [20] M. Varasteh, B. Rassouli, and B. Clerckx, "Wireless information and power transfer over an AWGN channel: Nonlinearity and asymmetric Gaussian signaling," in *2017 IEEE Information Theory Workshop (ITW)*. IEEE, 2017, pp. 181–185.
- [21] —, "On capacity-achieving distributions for complex AWGN channels under nonlinear power constraints and their applications to SWIPT," *IEEE Transactions on Information Theory*, 2020.
- [22] B. Clerckx and J. Kim, "On the beneficial roles of fading and transmit diversity in wireless power transfer with nonlinear energy harvesting," *IEEE Transactions on Wireless Communications*, vol. 17, no. 11, pp. 7731–7743, 2018.
- [23] X. Tan, Z. Sun, J. M. Jornet, and D. Pados, "Increasing indoor spectrum sharing capacity using smart reflect-array," in *2016 IEEE International Conference on Communications (ICC)*. IEEE, 2016, pp. 1–6.
- [24] S. Hu, F. Rusek, and O. Edfors, "Beyond massive MIMO: The potential of data transmission with large intelligent surfaces," *IEEE Transactions on Signal Processing*, vol. 66, no. 10, pp. 2746–2758, 2018.
- [25] Q. Wu and R. Zhang, "Intelligent reflecting surface enhanced wireless network: Joint active and passive beamforming design," in *2018 IEEE Global Communications Conference (GLOBECOM)*. IEEE, 2018, pp. 1–6.
- [26] S. Lee, Y. Zeng, and R. Zhang, "Retrodirective multi-user wireless power transfer with massive MIMO," *IEEE Wireless Communications Letters*, vol. 7, no. 1, pp. 54–57, 2017.
- [27] S. Shen, B. Clerckx, and R. Murch, "Modeling and architecture design of intelligent reflecting surfaces using scattering parameter network analysis," 2020.
- [28] X. Yu, D. Xu, and R. Schober, "MISO wireless communication systems via intelligent reflecting surfaces," in *2019 IEEE/CIC International Conference on Communications in China (ICCC)*. IEEE, 2019, pp. 735–740.
- [29] Q. Wu and R. Zhang, "Intelligent reflecting surface enhanced wireless network via joint active and passive beamforming," *IEEE Transactions on Wireless Communications*, vol. 18, no. 11, pp. 5394–5409, 2019.
- [30] H. Guo, Y.-C. Liang, J. Chen, and E. G. Larsson, "Weighted Sum-Rate Optimization for Intelligent Reflecting Surface Enhanced Wireless Networks," 2019.
- [31] C. Pan, H. Ren, K. Wang, W. Xu, M. ElKashlan, L. Hanzo, and A. Nallanathan, "Multicell MIMO communications relying on intelligent reflecting surfaces," *IEEE Transactions on Wireless Communications*, 2020.
- [32] B. Zheng and R. Zhang, "Intelligent reflecting surface-enhanced OFDM: Channel estimation and reflection optimization," *IEEE Wireless Communications Letters*, vol. 9, no. 4, pp. 518–522, 2019.
- [33] Y. Yang, S. Zhang, and R. Zhang, "IRS-enhanced OFDM: Power allocation and passive array optimization," in *2019 IEEE Global Communications Conference (GLOBECOM)*. IEEE, 2019, pp. 1–6.
- [34] C. Pan, H. Ren, K. Wang, M. ElKashlan, A. Nallanathan, J. Wang, and L. Hanzo, "Intelligent reflecting surface aided MIMO broadcasting for simultaneous wireless information and power transfer," *IEEE Journal on Selected Areas in Communications*, 2020.
- [35] Q. Wu and R. Zhang, "Weighted sum power maximization for intelligent reflecting surface aided SWIPT," *IEEE Wireless Communications Letters*, 2019.

- [36] Y. Tang, G. Ma, H. Xie, J. Xu, and X. Han, “Joint transmit and reflective beamforming design for IRS-assisted multiuser MISO SWIPT systems,” *arXiv preprint arXiv:1910.07156*, 2019.
- [37] Q. Wu and R. Zhang, “Joint active and passive beamforming optimization for intelligent reflecting surface assisted SWIPT under QoS constraints,” *arXiv preprint arXiv:1910.06220*, 2019.
- [38] H. Li, W. Cai, Y. Liu, M. Li, Q. Liu, and Q. Wu, “Intelligent reflecting surface enhanced wideband MIMO-OFDM communications: From practical model to reflection optimization,” *IEEE Transactions on Communications*, 2021.
- [39] B. Clerckx, “Wireless information and power transfer: Nonlinearity, waveform design, and rate-energy tradeoff,” *IEEE Transactions on Signal Processing*, vol. 66, no. 4, pp. 847–862, 2017.
- [40] T. Adali and S. Haykin, *Adaptive signal processing: next generation solutions*. John Wiley & Sons, 2010, vol. 55.
- [41] O. Mehanna, K. Huang, B. Gopalakrishnan, A. Konar, and N. D. Sidiropoulos, “Feasible point pursuit and successive approximation of non-convex QCQPs,” *IEEE Signal Processing Letters*, vol. 22, no. 7, pp. 804–808, 2014.
- [42] M. Grant and S. Boyd, “CVX: Matlab software for disciplined convex programming, version 2.1,” 2014.
- [43] Z.-Q. Luo, W.-K. Ma, A. M.-C. So, Y. Ye, and S. Zhang, “Semidefinite relaxation of quadratic optimization problems,” *IEEE Signal Processing Magazine*, vol. 27, no. 3, pp. 20–34, 2010.
- [44] W.-K. Ma, P.-C. Ching, and Z. Ding, “Semidefinite relaxation based multiuser detection for M-ary PSK multiuser systems,” *IEEE Transactions on Signal Processing*, vol. 52, no. 10, pp. 2862–2872, 2004.
- [45] W.-K. Ma, T. N. Davidson, K. M. Wong, Z.-Q. Luo, and P.-C. Ching, “Quasi-maximum-likelihood multiuser detection using semi-definite relaxation with application to synchronous CDMA,” *IEEE transactions on signal processing*, vol. 50, no. 4, pp. 912–922, 2002.
- [46] Q. Wu and R. Zhang, “Beamforming optimization for wireless network aided by intelligent reflecting surface with discrete phase shifts,” *IEEE Transactions on Communications*, vol. 68, no. 3, pp. 1838–1851, 2019.
- [47] H. Guo, Y.-C. Liang, J. Chen, and E. G. Larsson, “Weighted sum-rate optimization for intelligent reflecting surface enhanced wireless networks,” *arXiv preprint arXiv:1905.07920*, 2019.
- [48] V. Erceg, L. Schumacher, P. Kyritsi, A. Molisch, D. S. Baum, A. Y. Gorokhov, C. Oestges, Q. Li, K. Yu, K. N. Tal *et al.*, “IEEE P802. 11,” 2004.
- [49] B. Clerckx, K. Huang, L. R. Varshney, S. Ulukus, and M.-S. Alouini, “Wireless power transfer for future networks: Signal processing, machine learning, computing, and sensing,” *arXiv preprint arXiv:2101.04810*, 2021.
- [50] S. Boyd, S. P. Boyd, and L. Vandenberghe, *Convex optimization*. Cambridge university press, 2004.